DESIGN AND ANALYSIS OF MOSFET BASED ABSORBER FOR 5G MASSIVE MIMO BASE STATION

Thesis submitted for the fulfillment of requirements for the degree of

MASTER OF SCIENCE

in

Electronic Engineering

by

ELLIOT OSAHON OMORU

DEPARTMENT OF ELECTRONIC ENGINEERING, HOWARD COLLEGE, UNIVERSITY OF KWAZULU-NATAL, DURBAN - 4041 SOUTH AFRICA.

STUDENT NO.: 219096111   **APRIL 2021**

DESIGN AND ANALYSIS OF
MOSFET BASED ABSORBER FOR
5G MASSIVE MIMO BASE STATION

Student:

Elliot Osahon Omoru

Supervisor:

Prof. (Dr.) Viranjay M. Srivastava

This thesis submitted in fulfillment of the requirements

for the degree of Masters of Science: Electronic Engineering

in

Howard College of Agriculture, Engineering & Science

University of KwaZulu-Natal, Durban

South Africa.

As the candidate's supervisor, I have approved this thesis for submission.

Signed……………………………….....   Date: 9 April 2021

Name: Prof. (Dr.) Viranjay M. Srivastava

Declaration 1 - Plagiarism

I, **Elliot Osahon OMORU,** with Student Number **219096111** and the thesis entitled " Design and Analysis of MOSFET Based Absorber For 5G massive MIMO Base Station" hereby declare that:

(i)   The research reported in this thesis, except where otherwise indicated, is my original research work.

(ii)   This thesis has not been submitted for any degree or examination at any other university.

(iii)   This thesis does not contain other person's data, pictures, graphs, or other information unless specifically acknowledged as being sourced from other persons.

(iv)   This thesis does not contain other person's writing unless specifically acknowledged as being sourced from other researchers. Where other written sources have been quoted, then:

a. Their words have been re-written but the general information attributed to them has been referenced;

b. Where their exact words have been used, then their writing has been placed inside quotation marks and referenced.

(v)   Where I have reproduced a publication of which I am an author, co-author, or editor, I have indicated in detail which part of the publication was written by myself alone and have fully referenced such publications.

(vi)   This thesis does not contain text, graphics or tables copied and pasted from the Internet, unless specifically acknowledged, and the source being detailed in the thesis and in the references sections.

Signed…………………………………….   Date: 9 April 2021

(Elliot Osahon OMORU)

Declaration 2 – Publications

Details of contribution to publications that form part of the research presented in this thesis include publications in preparation, already submitted, in press and published. They give details of the contributions of each author to the experimental work, simulation and writing of each publication.

List of Publications

1 **Elliot O. Omoru** and Viranjay M. Srivastava, "Design and performance analysis of SiO_2-MOSFET based absorber for reflected RF signal," *Material Science Forum (MSF)*, vol. x, no. y, pp. xx-yy, 2021, selected from *3rd Int. Conf. on Materials Science and Manufacturing Technology (ICMSMT),* 8-9 April 2021.   ***[DoHET, SCOPUS]***

2 **Elliot O. Omoru** and Viranjay M. Srivastava, "MOSFET based absorber of reflected Signal in 5G massive MIMO base Station- A circuit perspective", *Journal of Communication*, vol. 15, no. 11, pp. 833-840, Nov. 2020   ***[DoHET, SCOPUS]***

3 **Elliot O. Omoru** and Viranjay M. Srivastava, "Simulation analysis of MOSFET based absorber for reflected RF signal in 5G massive MIMO base station*", International Journal of Emerging Trends in Engineering Research",* vol. 8, no. 251, pp. 6488-6495. Sept. 2020.   ***[DoHET, SCOPUS]***

Signed…………………………………….   Date: 9 April 2021
        (Elliot Osahon OMORU)

ACKNOWLADGMENTS

My sincere appreciation goes to my supervisor Professor Viranjay M. Srivastava for his patience, guidance, support, advice, time, and enthusiasm to undertake this research which has aided my thorough understanding of the study and the great flexibility and freedom he granted me in realizing the research objectives.

My sincere appreciation goes to my beloved mother, Patience O. Ewansiha, for her kindness, patience, support, understanding and encouragement all these years, you are indeed God sent. Thank you for your contribution towards my achievements. I also appreciate lovely Siblings Wisdom O. Ewansiha, Olaye Cynthia, Osayamwen Rita, Osayamwen Mathew, Idusogie Lilly, Mr Osamudiamen Osayamwen, Mrs Idemudia, and the children of Mr. Wilfred Osayamwen for their support.

I would like to express my appreciation to my postgraduate colleagues especially, Mr. Philip Smith of University of KwaZulu-Natal for sharing with me generously his academic experience and encouragement during the course of this study. Also, I will not forget to mention my friends, Osasogie Edomwandagbon and Zwe Mzulwini, for their encouragements, support and sacrifices all through the duration of my master's degree program.

Finally, I give all glory and honour to the Almighty God for His infinite mercy, grace and strength I acquired to complete this research work.

Dedication

This thesis is dedicated to my mother, Ewansiha Patience and the entire Omoru and Osayanmwen family.

To God be the Glory.

ABSTRACT

The Fifth Generation (5G) technology suffers from a series of drawbacks ranging from the high cost of infrastructure development, replacement of old devices that may not be compatible with 5G, and losses within the 5G base station construct. During transmission, these losses have a negative effect on the overall performance and efficiency of transmission systems. The 5G massive-Multiple Input Multiple Output (MIMO) base station structure suffers from these losses. In addition, a loss experienced in the 5G technology is due to the reflection of signals from the receiver (Rx) branch connected to the circulators in the 5G massive-MIMO base station. Operators often specify that the worst-case reflections (return loss) over the system's operating frequency range must be *18 dB* lower than the signal transmitted into the system.

As feed systems become shorter and antenna systems are required to operate over broader frequency ranges, achieving an *18 dB* return loss may not be practical, most especially at *a* 5G frequency regime. This reflection loss experienced in the 5G massive-MIMO base station results from the Rx branch's unmatched load impedance with the source impedance of the Transceiver (T_X) branch.

However, this problem can be solved by designing a matched circuit between the T_X and R_X branch of the base station. But Engineers are often faced with the challenge of designing a matching network for impedance mismatch, most especially at high frequency. For this reason, an N-channel Metal Oxide Field Effect Transistor (MOSFET) connected to a circulator has been proposed as an alternative solution to the performance and efficiency reducing effects of reflected radio frequency signal. The proposed model has been presented by connecting the Tx branch, antenna, Rx branch, and the MOSFET to each of the assumed four-port circulator ports.

Two comparisons have been made between the source current and drain current of the MOSFET whenever there is a reflection from the base station's Rx branch, In this research, four case of reflection from the R_X branch of the base station have been examined at 28 Ghz to analyse the model's performance. Various performance parameters (Insertion loss, Reflection coefficient, Total Power Absorbed by MOSFET (TPAM), Total Power Lost to Rectifier (TPLR), S-parameter, efficiency, etc.) have been analyzed for the validity,

stability, and reliability of the proposed model. At worst case reflection from port-3 of the circulator, TPAM, TPLR and reflection coefficient have been observed to be *0.64 mW, 2.95 mW,* and *0.0001179.*

Comparisons have been made with existing RF absorber models using efficiency, insertion loss, frequency, RF power absorption level, and ease of implementation as a standard. The model has been observed to have an efficiency greater than *90 %*, an insertion loss more significant than *38 dBm* at a frequency of *28 GHz.*

TABLE OF CONTENTS

List of Figures

List of Tables

List of Abbreviations

AC	Alternating Current
AFSS	Absorbing Frequency Selective Surface
CMOS	Complementary Metal Oxide Semiconductor1
DC	Direct Current
EDGE	Enhanced Data Rate for GSM Evolution
EMI	Electromagnetic Interference
ETACs	European Total Access Communication System
FSS	Frequency Selective Surface
FMCW	Frequency Modulated Continuous Wave
GSM	Global System for Mobile Communication
GPRS	General Packet Radio System
HH1	Hot-Hole Injection
HSDPA	High-Speed Downlink Packet Access
HSUPA	High-Speed Uplink Packet Access
IC	Integrated Circuit
IP	Internet Protocol
ISM	Industrial Scientific and Mechanical
IMPATT	Impact Ionization Avalanche Transit-Time
LTE	Long Term Extension
MOS	Metal Oxide Semiconductor
MOSFET	Metal Oxide Semiconductor Field Effect Transistor
MMIC	Monolithic Microwave Integrated Circuit
MMIMO	Massive Multiple Input Multiple Output
NBTI	Negative Bias Temperature Instability
NMOS	N-Channel Metal Oxide Semiconductor
NMT	Nordic Mobile Telephony
PMOS	P-Channel Metal Oxide Semiconductor
PSO	Particle Swarm Optimization
RCS	Radar Cross-Section
RF	Radio Frequency
RFID	Radio Frequency Identification
RITV	Rectifier Input Terminal Voltage

RITC   Rectifier Input Terminal Current

RWSWR   Relative Voltage Standing Wave Ratio

R_X Receiver

SC   Source Terminal Current

STM   Spatio-temporal Modulation

TACs   Total Access Communication System

TE   Transposed Electric

TM   Transposed Magnetic

TL   Transmission Line

TMN   Tuneable Matching Network

T_X Transmitter

TPR1   Total Power Reflected at Port-1

TPR2   Total Power Reflected at Port-2

TPAM   Total Power Absorbed by MOSFET

TPLR   Total Power Lost to the Rectifier

VDMC   Voltage Drop Along MOSFET Channel

Chapter-1

INTRODUCTION

1.1 Background

Telecommunication started with the introduction of the first generation (1G) of technology, which had Nordic mobile telephony (NMT), Total Access Communication System (TACS), and European Total Access Communication System (ETACS) as its sub-technologies. These were analog systems with short distance coverage. The Second Generation (2G) of technology was introduced [1]. The 2G technology marked the beginning of digital signal processing having sub generations like Global System for Mobile Communication (GSM), a 2 G voice technology, General packet radio service (GPRS) a 2.5 G technology, Enhanced Data Rate for GSM Evolution (EDGE) a 2.75 G technology. These sub-technologies brought about increase in data rate from GPRS to EDGE , all categorized as the 2G of technology. The major difference between the GSM and GPRS is their mode of switching, the GSM is circuit-switched while the GPRS is packet-switched [2, 3].

As a result of the increase in demand for data, the Third Generation (3G) of technology was introduced, having Universal Mobile Terrestrial/Telecommunication (UMTS) as its main technology, providing a data rate to *384 Kbps*. The vision of 3G technologies is based on wireless services that integrate multimedia, packet switching, and wideband radio with higher spectral efficiencies than the 2G technologies. The sub-technologies under this generation of technology are the 3.5 G High Speed Downlink Packet Access (HSDPA) and 3.5 G High Speed Uplink Packet Access (HSUPA), 3.75G High Speed Packet Access Evolved (HSPA$^+$), and 3.9 G Long Term Extension (LTE). The HSUPA concentrated on the upload speed related to cloud computing, while the HSDPA concentrated on the download speed. All these sub-technologies of 3G were targeted at introducing the Fourth Generation (4G) of technology, which provides about *1 Gbp*s for stationary users and *100 Mbps* for mobile users [4-6].

The 5G technology eventually increases data speed to about *15 Gbps* or more, low latency, ten times less than 4G technologies, and more bandwidth for users [7-9]. This generation of mobile technology is important for technologies like wireless gaming, virtual reality, self-driving cars, etc. [10]. It will also bring into the full operation of

Internet Protocol (IP) version 6, providing billions of users with IP. The 5G technology uses spectrum in the existing LTE frequency range between *600 MHz* and *6 GHz* and the millimeter-wave between *24 GHz* and *86 GHz* [11, 12,]. Obviously, these are very high frequencies, which results in small propagation distance and small cell size due to short-wavelength at high transmit frequency. Due to the naturally poor propagation capabilities at high frequency, which result in small cell size, more antennas are cooperated into the base station structure to improve the base it's coverage performance [13, 14]. The system of putting a hundred antenna into the base station structure to improve is called massive-MIMO. The m-MIMO units are often several times more expensive than traditional radio units, this is due to the higher bill of materials cost (than traditional radios) and increased manual assembly effort during manufacturing to attach the 16 to 96 antenna elements onto the main antenna board.

Although the m-MIMO technology is very promising, the m-MIMO base station suffers from reflection loss between its T_X branch and R_X branch of its construct. To tackle this problem of reflection, a model was proposed by *Yoo et al.* [15] at a frequency of *24.5 GHz,* this model uses an asymmetric coupler with high isolation between the (Tx) and (Rx) ports. This quasi-circulator consists of quarter-wave transmission lines, which have an unbalanced characteristic impedance at the terminated port, which is purposely unmatched with the coupler's reference impedance. The port compensates for the asymmetric impedances of the coupler using the proposed design parameter. Because of its asymmetric structure and the unmatched port usage, the proposed circulator has been accurately designed to have high Tx–Rx isolation without increasing the signal losses between Tx and Rx paths at the operating frequency. An active quasi-circulator at *30 GHz* was designed and fabricated by *Chang et. al.* [16] at TSMC *0.18 μm* mixed-signal CMOS technology. The current-reuse technique was integrated with a common-source stage to form the quasi-circulator core with reduced power consumption. A three-port active circulator and an active quasi-circulator based on bridged-T networks were designed and fabricated by *Wang et. al.* [17] at standard *0.18 mμ* CMOS technology. An active quasi-circulator MMIC was designed and fabricated by *Shin et al*. [18] at standard *0.18 μm* CMOS technology. It combines the common-source, common-gate, and common-drain configurations to improve the isolation between ports and improved insertion loss.

Ayati et al. [19] have presented an adaptive circulator fabricated on a *0.13 μm* CMOS. Dinc and Krishnaswamy [20] analyzed a *28 GHz* magnetic-tree non-reciprocal passive

CMOS circulator based on Spatio-Temporal conductance modulation. All these proposed circulator designs could be used to isolate the T$_X$ branch from the R$_X$ branch to avoid the negative effect of reflected RF power.

Furthermore, an impedance matching circuit could also be a solution to the effects reflected radio frequency signal in base stations. A novel impedance matching method using multiport network analysis and the Particle Swarm Optimization (PSO) algorithm was proposed by *Jeon et. al* [21]. To evaluate the proposed method's accuracy and reliability, the real handset model was employed, and the target impedance matching was conducted. Good impedance matching results were obtained for the LTE band 8. The calculated results were in excellent agreement with target impedance, under the Relative Voltage Standing Wave Ratio (RVSWR) of 1.5. *Morikoshi et. al* [22] designed an onboard Millimeter-Wave matching circuit pre-system. These on-board impedance matching circuits were essential to suppress return loss in each RF module. The on-board impedance matching circuit was designed using different pre-existing models. Owing to these accurate models, the fabricated impedance matching circuit achieved a return loss smaller than *-10 dB*.

A varactor-based variable impedance matching network intended to be integrated into an automatic impedance matching system was designed by *Added and Boulejfen* [23]. This design's operating frequency was fixed at *2.4 GHz,* suitable for Industrial, Scientific and Medical applications (ISM). The design featured broad impedance coverage with a low reflection loss. The simulation results demonstrated the efficiency of the proposed design for narrowband applications.

1.2 Research Objectives

Some losses are currently being experienced, and more are anticipated in the 5G base station structure. One such loss is due to the reflection of RF signal from the Rx branch of base station because of impedance mismatch between the Tx branch and the Rx branch. To improve the 5G Massive MIMO base station's working, a model with MOSFET has been used to absorb the reflected signal from the circulator [24-26]. Using a four-port circulator to carry out both duplexing and isolating functions within the base station, the Tx branch, Rx branch, MOSFET, and the transmit-receive antenna (transceiver) branch are connected to each port of the circulator.

Comprehensively, the proposed model's expected performance has been defined and computed using technical parameters like insertion loss, efficiency, reflection coefficient, and other performance parameters have been calculated. Additionally, a comparison has been made with the existing RF absorber model.

1.3 Significance of Research.

From this research work, an absorber model that can easily be implemented and operated at a very high frequency has been designed, specifically at 5G frequencies, where efficiency at the highest level of constraints is the major target of telecom companies. This model has proven to be highly efficient in terms of the level of absorption they can provide, compared to other existing absorber models. In addition to this, the model has proven to be a solution to Engineers' challenges during the design of impedance matching circuits for base stations. Furthermore, for optimum performance in 5G regime of technology, the SiO_2 MOSFET have been observed to be a solution to the resultant effect of arching within the transmission line under large field intensities of standing wave resulting from impedance in consistency or mismatch. Also, in the future generations of technology, the proposed model will still be effective because modification of design only involves designing the proposed model circuit to suite the frequency of existing regime of technology.

1.4 Methodological Approach

As a result of the lack in the model for simulating a real circulator port, a sinusoidal voltage source has been used to provide an equivalent source or T_X branch terminal voltage component of incident RF power on port-2. With the help of a voltage divider, the equivalent voltage component of reflected RF power from port-3 of the circulator (R_X branch) has been generated and applied to the rectifier's input terminal connected to an assumed port-4 of the proposed model construct. At the rectifier's output terminal, an N-channel MOSFET has been connected to absorb the resulting output power from the rectifier output of the proposed model construct. Though the power level representing the reflected signal from the receiver port is very large, which may result in saturation of the receiver, these values of incident power on port-2 and reflected power from the Rx branch, have been chosen for testing and experimental purpose to verify the consistency of the model.

Furthermore, to verify the consistency of the model parameters, the values of the current and voltage at the output terminal of the MOSFET have been compared with the values of the voltage and current at the input terminal of the rectifier to determine the level of absorption of the proposed model at a 5G frequency of *28 GHz* under *43 dBm* transmit power, incident on an assumed port-2 of a circulator.

However, on the proposed model's physical implementation, a real circulator port and a high-frequency Schottky diode and distributed circuit will be employed for the rectification process because when frequencies are too high, it becomes difficult for discrete capacitors and inductors to be practical.

1.5 Thesis Organization

This thesis is organized as follow:

Chapter 1 gives a brief history of telecommunication, starting from the 1G of technology 5G of technology. It also summarizes challenges faced in the latest 5 G technology and how some previously designed models could be a solution to the specific challenge under discussion.

Chapter 2 has a brief analysis of wireless technology, advantages and challenges, and existing solutions to tackle the problem that could arise whenever there is a reflection from the R_X branch of the base station. It also analyses the working principles of the various component used for the proposed model construct. An analysis of existing absorber models, the insertion loss they can provide, and the frequency at which they can be operated have been captured in this chapter.

Chapter 3 presents a circuit perfective of the proposed model- MOSFET Based Absorber of Reflected RF power in 5 G massive MIMO base station. Thereafter, two comparisons have been made between the source current and drain current of the MOSFET whenever there is a reflection from the base station's Rx branch.

Chapter 4 has the simulation analysis of the proposed model, and its workings are presented. It focuses on examining the consistency of the parameters and theories used for the MOSFET-based absorber under different reflection conditions from circulators' ports in 5G base stations.

Chapter 5 has a design and performance analysis of the proposed model is presented. Various performance parameters (Gain, Reflection coefficient, total power absorbed by MOSFET, S-parameter, efficiency, etc.) have been analysed for the validity, stability, and

reliability of the proposed model. In addition to this, the comparison has been made with existing models using efficiency, RF power absorption level, and ease of implementation as a standard for comparison.

Chapter 6 discusses the results of the proposed model, the advantages and the disadvantages. It also gives a brief analysis of the physical implementation of the proposed model.

1.6 List of Publications

1   **Elliot O. Omoru** and Viranjay M. Srivastava, "Design and performance analysis of SiO_2-MOSFET based absorber for reflected RF signal," ***Material Science Forum (MSF)***, vol. x, no. y, pp. xx-yy, 2021, selected from *3rd Int. Conf. on Materials Science and Manufacturing Technology (ICMSMT),* 8-9 April 2021.   ***[DoHET, SCOPUS]***

2   **Elliot O. Omoru** and Viranjay M. Srivastava, "MOSFET based absorber of reflected Signal in 5G massive MIMO base Station- A circuit perspective", *Journal of Communication*, vol. 15, no. 11, pp. 833-840, Nov. 2020   ***[DoHET, SCOPUS]***

3   **Elliot O. Omoru** and Viranjay M. Srivastava, "Simulation analysis of MOSFET based absorber for reflected RF signal in 5G massive MIMO base station*", International Journal of Emerging Trends in Engineering Research",* vol. 8, no. 251, pp. 6488-6495. Sept. 2020.   ***[DoHET, SCOPUS]***

1.7 Conclusion

A brief history of telecommunication, starting from the first generation of technology to the fifth generation of technology have been presented. Also, a summary of the possible solution to the challenges of the latest 5G of technology have been presented. Furthermore, the objective, significance and thesis organization have been systematically analysed in this chapter.

Chapter-2

LITERATURE REVIEW

2.1   Wireless Communication

Wireless communication has existed in various generations starting from the first generation of wireless technology, where Guglielmo Marconi successfully demonstrated a Wireless Telegraph in the year 1987. This demonstration paved the way for future generations of wireless technology, including the present 5G of technology. The term Wireless communication is a general word that integrates all types of wireless communications and networking between two or more devices using a wireless signal [27, 28]. Although wired communication could do most of the activities wireless communication can do, immobility and infrastructure cost are its major constraints.

With powerful features, the advent of wireless technology has brought many significant advances in technology over the past few decades. It has also become one of the most important media transmission types from one device to another [29]. In addition to this, for effective wireless communication between devices using electromagnetic waves, the antenna is the most important component. This component consists of a group of metal conductors connected to a transmitter and a receiver. It covers electrical current moving in a metal conductor into an electromagnetic wave or otherwise.

In various branches of wireless communications, there is a broad range of antennas used. The simplest and most widely used antennas are wired antennas used as a dipole, circuit, or helical antennas. The open antennas in the form of horns or mirrors are another significant type of antennas. Array antennas are commonly used as switched beam antennas or adaptive antennas in communications [30, 31]. This component's performance can be analysed using parameters such as radiation patterns, directivity, gain, polarization loss, etc.

2.1.1 Advantage of wireless communication

Wireless communication technology provides various advantages over the use of wired communications. Mobility is the main advantage of a wireless communication system. It offers the freedom to move around while still connected to a network. Also, with

wireless, the cost of building wires, cables, and other equipment is reduced compared with the wired communication system. Another key advantage of wireless technology is the ease of installation, configuring, and installing the wireless communication network's equipment and infrastructure is very simple, so cables are not a problem to think about. In contrast to the setup of a complete cabled network, the time needed to install a wireless device such as a Wi-Fi network is quite small [32]. Additionally, since wireless communication is not subject to cables and wires, the damage of those cables, resulting from environmental conditions, cable splices, and natural decreases in metallic conductors, will cause no communication loss.

Although device to device communication without wires' use may have a lot of promising advantages over wired communication, it has its challenges.

2.1.2 Challenges of wireless communication

Wireless communication is primarily concerned with data protection. Since the signals are transmitted in open space, the signals may be a captured and confidential information copied by an attacker [33]. Also, many health concerns have been raised regarding wireless for the device-to-device communication. There could be harmful, ongoing exposure to some form of radiation. While RF energy levels, which through because harm is not reliably calculated, RF radiation should be avoided as far as possible [34].

Furthermore, one major challenge currently being experienced in wireless communication is the negative effect of signal interference during transmission and reception, most especially in the MIMO base station construct [35-37]. Various work has been done to reduce the effect of interference in the base station, especially interference resulting from the signal from the R_X branch of the MIMO base station. This problem could be solved using matching circuits between the T_X branch and R_X branch of the base station or simply using a Circulator to isolate the R_X branch from the T_X branch.

To reduce the effect of reflection, the simplest network for matching a load resistance R_L to a source resistance R_S (T_X branch resistance) at a single frequency was analysed by *Roy* [38] to find the matching expression bandwidth with a specified tolerance on the reflection coefficient. *Jurkov et. al* [39] developed a Tuneable Matching Network (TMN) that enables a combination of much faster and more accurate impedance matching than is available with conventional techniques and is suitable for use at high power levels. Since designing a compact, active quasi-circulator was proposed and experimentally

demonstrated by *Sheng and Saavedra* [40]. It consists of an active balun and a current combiner using operational transconductance amplifiers in CMOS. The proposed model was designed to operate at a frequency of *1.5-2.7 GHz*. Though designing an impedance matching circuit could be a solution, engineers are faced with the challenges of designing a matching circuit, especially in present-day 5 G wireless communication.

2.2 Circulators and Principles of Operation

The discovery of a simple, low loss way to hold Faraday rotation constant over broadband (coupled with the development of wideband, high return loss, circular-to-rectangular waveguide transformers, and polarization couplers) has made it possible to design and build a high-quality RF circulator [41]. RF circulators are passive components essential to modern communication systems. They act as traffic routers for RF signals, moving them to any place in the circuit.

Also, an RF circulator is a non-reciprocal three or four-port device used to regulate signal flow within a circuit. Power is transferred from one port to the adjacent port in a prescribed order. The device is non-reciprocal means their behavior in one direction is different from their behaviour in another direction. It is a device used for transmission in which microwave or radio-frequency signal entering any port are passed on to the next port in rotation only. In this context, a port is a point where an external waveguide or transmission line is connected to the device.

2.2.1 Types of Circulators

Depending on the materials used for the design and fabrication, circulators fall into two main categories:

- Ferrite circulators
- Non-ferrite circulators

A. Ferrite Circulators

These are radio frequency circulators fabricated with anisotropic magnetic material (ferrite). Anisotropic materials exhibit different electrical characteristics that depend on how the electrical signal moves the magnetized ferrite. The microwave ferrite circulator is a non-reciprocal device used as an isolator or duplexer in a microwave system or as a shared device for microwave communications and transceivers [42,43]. The major

problem with this type of circulators is the fact that, because of the need for a magnet for their operation, they are too big to fit in today's very small electronic devices, like wearable, or in systems like the coming 5G networks, self-driving cars or virtual reality systems.

A microstrip ferrite circulator was designed by *Hao et. al.* [44]. This microstrip ferrite circulator's working principle was derived from the strapline circulator, having a typical structure of a strapline, with three metal strip lines symmetrical with each other at 120 degrees and in the two ground planes. A ferrite columnar substrate was disposed between each and was prepared by applying a bias magnetic field with suitable strength. This microstrip circulator was designed to work at a frequency of *1.9-2.6 GHz*. The design of this microstrip circulator was mainly based on the Busman's circulation conditions. A modelling approach for designing micro strip ferrite circulators was presented and validated on several examples by *Pinto et. al*. [45]. A baseline narrowband *4.25 GHz* microstrip circulator was demonstrated with a commercial *4.97 mm* radius ferrite disk operated in saturation and below the ferromagnetic resonance. The non-uniform DC magnetic field distributions of a cylindrical permanent magnet were considered by spatial discretization of the ferrite properties in full-wave simulations. Several design parameters were shown to affect the frequency response; the ferrite thickness relative to the microstrip substrate thickness shifts the operating frequency, while external matching networks increased the fractional bandwidth from *10 %* up *40 %.*

B. Non-Ferrite Circulators

Early days of this type of circulator included an active circulator using transistors that are non-reciprocal in nature in contrast to the ferrite circulators that use anisotropic magnetic material. Also, these types of circulators are energetic circulators thus, they need extra power. An example of this type of circulator was proposed by *Krishnaswamy* [46]. This circulator was created to operate at millimeter frequencies and were built into semiconductor chips. This allows two-way (duplex) wireless communication in which a transmitter and a receiver operated simultaneously on the same channel and frequency. This doubles the data-rate within the existing bandwidth. This mm-wave circulator enables mm-wave wireless full-duplex communications, which could revolutionize emerging 5G cellular networks, wireless links for virtual reality, and automotive radar.

As proof of the recently introduced concept of Spatio-temporal modulation (STM) to efficiently implement angular momentum biasing, which is a biasing technique that breaks the time-reversal symmetry yielding a non-reciprocal response, a non-ferrite circulator was designed by *Nafe et. al.* [47] at *500 MHz*, and demonstrates a *15 dB* isolation fractional bandwidth of *8.5 %,* insertion loss of *3.9 dB*, and return loss of better than *13 dB*. *Dinc et. al.* [48] presents a detailed analysis of the millimeter-wave circulator in both time and frequency domains. Millimeter-wave non-reciprocal operation is enabled by the concept of Spatio-temporal conductivity modulation, which achieves broadband non-reciprocal gyrator functionality over theoretically infinite bandwidth (BW).

2.2.2 Function of a Circulator

The non-ferrite and ferrite circulators can be designed to function as a duplexer, isolator or designed to perform both operations.

A. Circulator as a Duplexer

An RF Duplexer is an electronic device used in RF communications transceiver circuits to share the same antenna. This is important because transmitters are large signal devices, and receivers are extremely sensitive small-signal devices. Without a duplexer to isolate the receiver and transmitter with low insertion loss for the antenna to the receiver, the transmitter overloads and most often damages a receiver if they share the same antenna. A Metal Oxide Semiconductor (MOS) circulators/duplexer based on non-reciprocal Transmission Line (TL) was proposed by *Yang et. al*. [49] for full-duplex transceiver front ends operating at *100 GHz* band. Offering non-reciprocal propagation at the millimeter-wave regime, the presented non-reciprocal TL is made of two parametric mixing stages modulated by signals at around *1/6* of the RF frequencies.

Operating together with integrated hybrid couplers, circulators, or duplexers can be implemented for full-duplex communication. Realized in the CMOS process, this non-reciprocal TL achieves over *45 dB* isolation throughout its isolation bandwidth of *1.5 GHz*, a maximum *9.5 dB* Insertion Loss (IL), and an over 10 dB return loss. A passive circulators/duplexer for Radio Frequency Identification (RFID) applications in the Ulta High Frequency (UHF) band was designed by *Leisten et. al.* [50]. The design idea is based on the use of simple passive directional couplers, offering simplicity and low cost

compared to ferrite devices or active architectures. The T_X/R_X isolation problem was solved by a mismatched load, which creates a canceling signal on the Rx port.

B. Circulators as an isolator

The unidirectional properties of microwave isolators are useful for protecting the output of load-sensitive devices against unwanted reflections. For example, the inclusion of an isolator at the oscillator's output serves to protect it from load pulling. A base theory and design approach for mag-netless isolators using grounded transistors was presented by *Barradas et. al.* [51]. This magnet-less isolator design with *20 dB* isolation and *3 dB* insertion loss at a frequency of *2.1 GHz*. Non-reciprocal components have found extensive use in radio frequency applications. Because of the difficulty in integrating these components, keen interest has been created for non-reciprocal components and structures not dependent on any magnetic components.

Ghaffar et al. [52] presented a novel half mode waveguide-based ferrite isolator design with the isolation band's tunability was demonstrated for a ferrite isolator. Instead of using the conventional antisymmetric bias, the isolator requires a single direction of the magnetic bias field due to the half mode operation. The principle of operation of the proposed isolator is analyzed numerically, and the obtained low losses originate from the wave transmitted in the gap. This behaviour is also demonstrated using the prototype of this type of isolator working at *6.25 GHz*, were simulated and measured results show the isolation of *48 dB* and insertion losses of *1.3 dB*. *Marynowsk et al.* [53] presented an integrated broadband edge-guided mode isolator with the ferrite slabs' antiparallel biasing. The principle of operation of the proposed isolator was analysed numerically, showing a specific behaviour. This behaviour was also demonstrated using the prototype of this isolator working at a frequency of *6.25 GHz*. The simulated and measured results show the isolation of *48 dB* and insertion losses of *1.3 dB*.

2.2.3 Application of Circulators

Isolators and duplexers have application in:

- Reflection amplifier design
- Radar systems
- Amplifier systems
- Antenna transmitting and receiving system

A. Circulators in the Design of Reflection Amplifiers

Reflection amplifiers were common up until the '80s, implemented mostly with Impact Ionization Avalanche Transit-Time (IMPATT) diodes, and were used as a building block for high-frequency amplifiers incorporated with circulators in order to implement a standard 2-ports amplifier. However, they are barely used nowadays in 2-ports configuration, thanks to advances in semiconductor technologies [54]. A circulator's work in the reflection amplifier separates the reflected incident signal in any RF system [55].

B. Circulators in Transmitting or Receiving Antenna and Radar Systems

The isolation of a weak receiving (R_X) signal from a strong transmitting signal (T_X) is one of the main functions of transmitting and receiving a single antenna module. The functionality is commonly implemented using passive devices in the state-of-the-art Frequency Modulated Continuous Wave (FMCW) and radar Monolithic Microwave Integrated Circuit (MMIC), with relatively broad physical dimensions compared to a chip region and exhibit insertion loss. An active quasi-circulator was designed by *Porranzl et. al.* [56] at *77 GHz* automotive FMCW radar systems in Silicon-Germanium (SiGe) technology. The active QC implemented is designed in a *200 GHz* f_T heterojunction bipolar transistor (HBT) technology. The measurements on-wave show *16 dB* of T_X/R_X isolation over an 8 GHz bandwidth. The T_X and R_X signal insertion losses calculated are respectively below *1 dB* and *1.5 dB*. *Nakamoto et. al.* [57] proposed a model for measuring the amplitude and phase relationship between the antenna mode and the structural mode for the deterministic Radar Cross-Section (RCS) reduction. The proposed method's efficacy was tested by experiments using an array antenna with circulators and optical phase shifters.

2.2.4   Characteristics of circulators

The three main characteristics of circulators and isolators are "Insertion loss (forward loss)," Isolation loss (reverse direction loss)," and VSWR. Since circulators have frequency characteristics, we must specify a particular frequency range when using the circulator. All these characteristics are needed for the proper functioning of the circulator.

A. Insertion Loss

Insertion loss is a circulator characteristic that reflects negatively on the performance of the circulator. Insertion loss causes a mismatch between the transmitter and receiver

due to power loss in the transmitted signal. This loss occurs when a signal passes through an insertion portion or device. It is expressed in (dB) and given by [58].

$$Insertion\ Loss\ (dB)\ =\ 10\ \log\left(\frac{P_{in}}{P_{out}}\right) =\ -10\ \log\left(\frac{P_{out}}{P_{in}}\right) \tag{2.1}$$

where P_{in} and P_{out} are input power and output power, respectively.

B. Voltage Standing Wave Ratio (VSWR)

The VSWR is described in a standing wave pattern as the ratio of maximum voltage to minimal voltage along with the structure of the transmission line or a microwave device. It ranges between 1 and infinity. This value is always positive, a number, the VSWR of a circulator is given by [59].

$$VSWR\ =\ \frac{1+\sqrt{\dfrac{P_{ref}}{P_{fwd}}}}{1-\sqrt{\dfrac{P_{ref}}{P_{fwd}}}} \tag{2.2}$$

Also, VSWR can be expressed as a function of the Reflection coefficient (Γ). The reflection coefficient is a parameter that describes how much of an electromagnetic wave is reflected by an impedance discontinuity in the transmission medium.

$$VSWR = \frac{1+\Gamma}{1-\Gamma} \tag{2.3}$$

$$\Gamma = \frac{Z_L - Z_0}{Z_L + Z_0} \tag{2.4}$$

where Z_0 and Z_L are the source and load impedance, respectively.

C. Isolation

This is a measure of the signal levels at the circulator's neighbouring ports, i.e. when a signal occurs at port one and is transmitted to port 2, the isolation is determined between port-1 and port-3. The higher the rating, the better the output of the circulator. It is measured in decibel (dB).

2.2.5 Principle of Operation of a Circulator

In this present research work, the circulator has been constructed with the use of two magic tees, each having four ports connected by a phase shifter [60-62]. The circulator is

constructed using two magic Tees, each of these magic tees has four ports. The magic tee is an 180^0 hybrid power divider that could be utilized as a power divider or a power splitter. The magic tee is made up of two collinear arms, the H-arm and the E-arm. The magic tees are placed parallel to each other, and the port-2 of each of the magic tees are connected via a micro strapline, and port 1 of the two magic tees are linked via an 180^0 phase shifter as shown in further subsections. This phase shifter could either be digital, analogue, or mechanical.

A. Case – 1 (Port-1: in, port-2: out)

As shown in Fig. 2.1 through port-4 of the magic tee-2, which is the port-1 of the circulator, Applying an input signal, splits into two signals of equal magnitude and the same phase. These signals go out through port-1 and port-2 of magic tee-2 and travel to port-1 and port-2 of magic tee-1. They enter into port-1 and port-2 of magic tee-1, maintaining the same phase. Though the signal from port-1 of magic tee-2 crosses an 180^0 phase shifter before it enters port-1 of magic tee-1, its phase remains the same because the power shifter works in one direction. Since signals entering port one and two of magic tee1 are in the same phase, they recombine and go out through port4 (H-arm) of magic tee-1, which happens to be the port-2 of the circulator. They go out through the H-arm because the condition for outputting a signal states that whenever two signals combining to produce an output are in the same phase, their output must always go out through the H-arm of the magic tee. In this case, the magic tee-2 acts as an RF splitter, while the magic tee1 acts as an RF combiner.
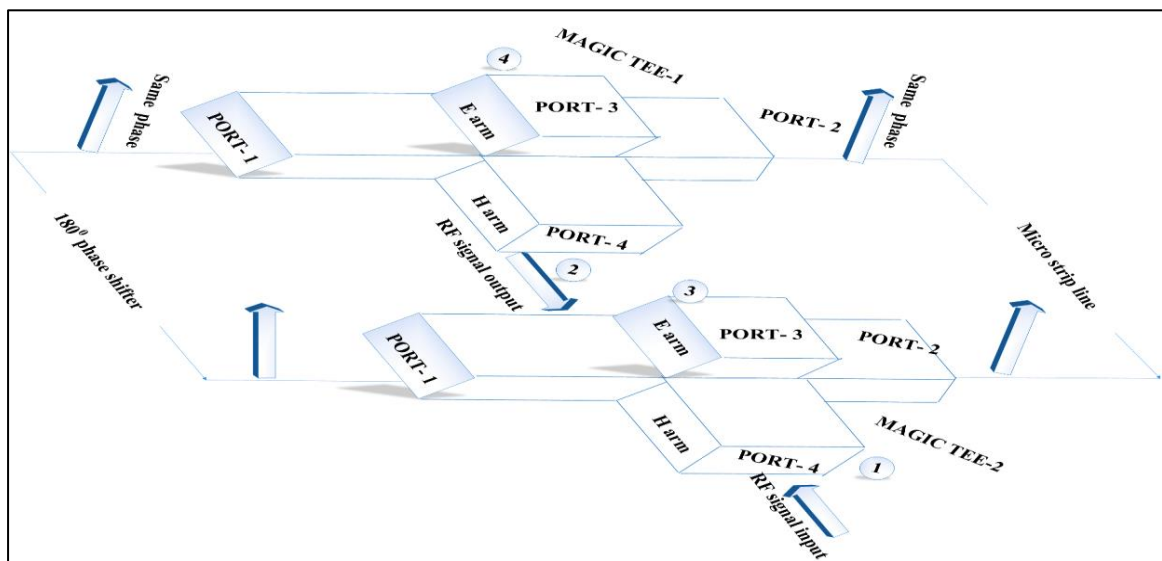
Fig. 2.1   Port-1 is for in and port-2 is for output.

B. Case – 2 (Port-2: in, port-3: out)

Applying input signal as shown in Fig. 2.2 through port-4 of magic tee-1, which is the port-2 of the circulator, splits into two signals of equal magnitudes and the same phase, these signals come out from port-1 port-2 of magic tee-1 and move towards and move towards magic tee-2. Signals from port-2 of magic tee1 enter port-2 of magic tee-2 maintaining the same phase and magnitude, signals from port-1 of magic tee-1 experience a phase shift and changes its phase as it enters port-1 of magic tee-2. The signals at port-1 and port-2 of magic tee-2 are equal in magnitude but opposite in phase. Recall if the inputs are of opposite phase, the signal will go out through the E arm of magic tee-2, which is the port-3 of the circulator. In this case, the magic tee-2 is functioning as a combiner of the radio-frequency signal while the magic tee-1 is functioning as a splitter of RF signal.
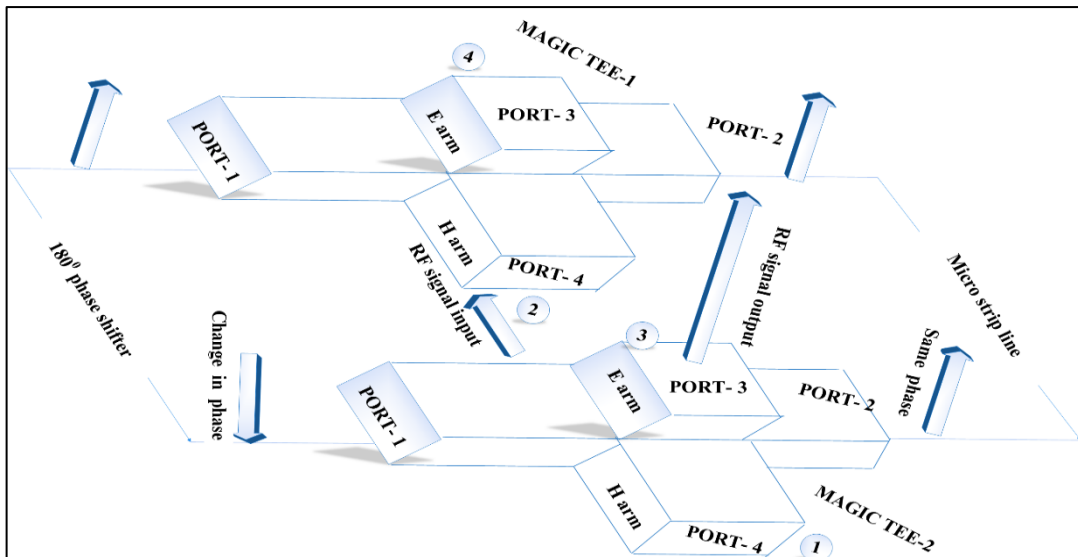
Fig. 2.2. Port-2 is for in and port-3 is for output.

C. Case – 3 (Port-3: in, port-4: out)

Applying an input signal as shown in Fig. 2.3 through port-3 (E-arm) of the magic tee-2, it splits into two signals of equal magnitude opposite phase. These signals come out through port-1 and port-2 of magic tee-2 and move towards the port-1 and port-2 of magic tee-2, maintaining the same split magnitude and phase at which they came out of the ports of magic tee-2. Though the signal from the port-1 of magic tee-2 encounters an 180^0 phase shifter, the signal phase does not change because the phase shifter works in only one direction.
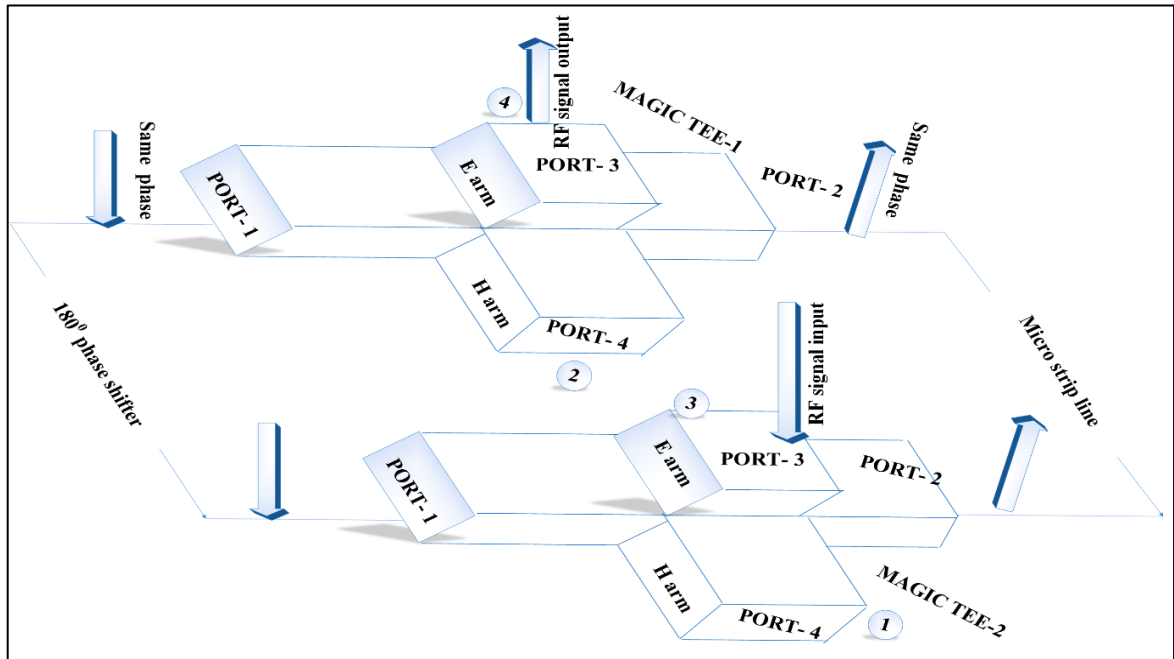
Fig. 2.3. Port-3 is for in, and port-4 is for output.

Now, signals entering into port-1 and port-2 of magic tee-1 recombines and comes out through port-3 (E-arm) of magic tee-1, the port-4 of the circulator. This is because whenever signals move in opposite phase, they always go out through the E-arm. In this case, the magic tee-1 acts as a radio frequency signal combiner, while the magic tee-2 acts as a radio frequency signal splitter.

D. Case – 4 (Port-4: in, port-1: out)

Applying an input signal as shown in Fig. 2.4 through port-3 (E-arm) of magic tee-1, which is the port-4 of the circulator, the signal splits into two signals of equal magnitude and opposite phase. Note they now have opposite phases because they are coming through the E-arm. The signals will come out from port-1 and port-2 of the magic tee-1 and move towards port-1 and port-2 of magic tee-2. The phase of the signal from port-2 of magic tee-1 remains the same as it gets to port-2 of magic tee-2, but the phase of signals from port-1 of magic tee-1 changes as it crosses the 180^0 phase shifter. The resulting signals of port-1 and port-2 of magic tee-2 have the same magnitude and same phase. Recall that when signals are in the same phase, they combine and come out through the H-arm. In this case, port-1 and port-2 signals tee-2 combine and come out as output through port-4 (H-arm) of the magic tee-2, which is the port-1 of the circulator.
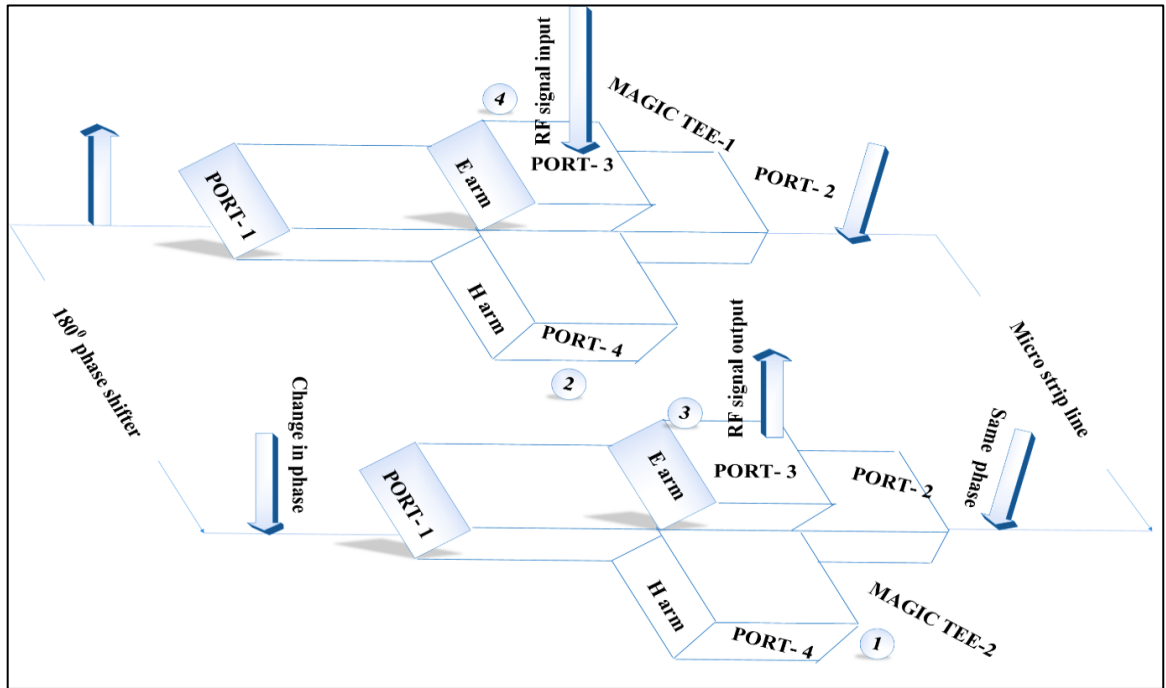
Fig. 2.4 Port-4 is for in and port-1 is for output.

The S matrix for a four-port circulator is represented as:

$$\mathbf{S} = \begin{pmatrix} s_{11} & s_{12} & s_{13} & s_{14} \\ s_{21} & s_{22} & s_{23} & s_{24} \\ s_{31} & s_{32} & s_{33} & s_{34} \\ s_{41} & s_{42} & s_{43} & s_{44} \end{pmatrix} = \begin{pmatrix} 0 & 0 & 0 & 1 \\ 1 & 0 & 0 & 0 \\ 0 & 1 & 0 & 0 \\ 0 & 0 & 1 & 0 \end{pmatrix}$$

At 5G frequencies, the concept of voltages and currents become difficult when analyzing circuit performance. S matrix or S parameters are used to overcome the problem that could have occurred when H, Y, Z and A, B, C, and D parameters characterize the circuit performance at high frequencies. Furthermore, Z, H, Y AND A, B, C, D cannot be measured at microwave frequencies because the equipment is not readily available to measure total voltage and current at the circulator port. For these reasons, the S matrix of a four-port circulator was generated for the proposed model.

2.3 RF Absorbers

Historically, armed forces in countries have used microwave absorbers to reduce high-frequency power reflections. Over time, the use of these products has evolved such that they are now often used in many industrial applications, including wireless communication devices, computer devices, and wireless antenna systems. This usage results from the difficulty in controlling radiation from the reflection in a high-frequency circuit or device.

To gain control, RF/microwave absorber materials are often applied to circuits to reduce or remove unwanted radiation from the circuit to the outside or to mitigate the effects of radiated signals outside the circuit on circuit output [63]. Absorber materials are described by parameters such as magnetic loss of tangent, speed of RF propagation, reflectivity, permittivity, and permeability of the absorber material, which differ dramatically in frequency [64, 65]. Absorber materials are either wide or more broadband in nature.

Furthermore, these absorber materials are available in various formats and are designed to absorb RF signals at a specific frequency [66]. Different materials have different attenuation levels for this purpose, the following criteria must be considered when choosing an RF absorber.

2.3.1 Configuration of the absorber

This can best be described as the form factor of the absorbing material used for the absorber design [67]. It can exist in the form of a pyramid, wedge, or any shape. They can be configured using the following parameters:

A. Frequency

This is the frequency range to which signal absorption is expected. Various materials are designed for specific frequency ranges. Also, frequency ranges can be combined to realize enhanced bandwidth absorption. This was demonstrated by *Ghosh and Srivastava* [68] with the use of dual-band switchable absorbers.

B. Attenuation

This is the level of absorption that the material can provide. It is usually measured in *dB*. Better microwave absorption and a good surface wave attenuation performance are very important characteristics to look out for when selecting an absorber, most especially those desired for usage in a wide frequency range [69, 70]. Also, the amount of attenuation of the microwave is dependent on the frequency and the electrical dielectric constant, and the magnetic permeability of the material.

2.3.2 Types of absorbers

RF absorbers are of two types, the dielectric type in which absorbing fillers act on the electric fields and the magnetic type in which the absorbing fillers act on the magnetic field. These absorber types have a high emissivity in the microwave range and are critical

in a wide range of applications, including avoidance of electromagnetic interference, stealth technology, and microwave radiometers [71, 72].

These absorber types could be classified as broadband absorbers or narrowband absorbers depending on the frequency range they can effectively attenuate. The broadband absorbers function over a wide frequency range, but typically, the level of attenuation is small, while the narrow band absorbers provide a high level of attenuation but can function effectively in a shorter range of frequency [73].

Although most absorbers exist in the above forms, they could also take the form of analog circuits, depending on the frequency requirement and the level of absorption they can provide [74].

2.4 Existing Absorber Models

Various engineers have presented absorber models to tackle the problem of signal interference from reflection or any other source. A new miniaturized absorber frequency selective surface for low-frequency transmission/high-frequency absorption was designed by *Hu et. al*. [75]. This design consists of two parts, with the upper layer of the design providing a *12 GHz to 18 GHz* absorbing band and an absorption rate is greater than 90 %. In the lower layer, the symmetrical frequency's selective region is below *1.8 GHz*, and the wave transmission rate is more than *84 %*. Han *et. al* [76] proposed a wave-Absorbing Frequency Selective Surface (AFSS) with low-frequency transmission/high-frequency absorption. The proposed model improved radar stealth by reducing the RCS of the antenna system without affecting the radiation performance. The unit adopts the method to load the frequency selection structure proportional to the absorber metal reflecting surface so that the frequency selection feature does not influence the effect of the absorption of the microwave. The proposed model provided an insertion loss greater than *10 dB* at a frequency of *4 GHz* to *5.5 GHz*. Using equivalent circuit analysis, an absorber design was proposed and optimized for C-band by *Saikia et. al*.[77]. The design consists of a capacitive layer and a circuit analog layer with lumped resistors. The built microwave absorber's complete wave simulation reveals a bandwidth below *-10 dB* absorption in *4.23 GHz* to *8.13 GHz*.

Additionally, a grapheme absorber was proposed using frequency selective surface (FSS) and resistive graphene strips on a grounded dielectric slab by *Fu et. al*. [78]. The basic circuit model shows that two adjacent absorption bands can be achieved by

combining loops with different substrate thicknesses. The proposed model is designed to operate at a frequency of *9.5 GHz to 55 GHz.* A similar model was proposed by *Kundu et. al* [79] with the use of the Impedance Analysis Method of the Equivalent Circuit Model. The proposed impedance analysis also helps to understand the absorption mechanism of conductive FSS based ultrathin absorbers. It provided an insertion loss of less than *15 dB* at an operating frequency of *5.9 GHz. Doken et. al.* [80] designed a Simple Frequency Selective Absorber Surface at a frequency of *2 GHz* to *7 GHz.* This was achieved by comparing it with the Salisbury absorber. This absorber's performance is maintained over wide incidence angles (0 to 45 degrees) and for both Transposed Electric (TE) and Transposed Magnetic (TM) polarizations.

Furthermore, broadband and switchable absorber using an absorb/reflective FSS was designed by *Guo et. al* [81], this absorber is composed of a conductive FSS square ring centred on the dense, low-loss substratum *λ0/32*. The absorber was manufactured to verify the simulating circuit result of the equivalent model and full-wave simulation result. It was observed to produce an insertion loss of less than *10 dB* at a frequency of *2.5 GHz* to *5.5 GHz.* A design and analysis of a broadband single layer circuit analog absorber was presented by *Ghosh et. al*. [82], the proposed absorber consists of a periodic arrangement of square loops loaded with lumped resistors, which exhibits *10-dB* bandwidth from *7.56 GHz* to *14.58 GHz* under normal incidence, covering X and Ku bands. Also, a design and measurement of a planar Radom absorber under oblique incidence are presented by *Hamid et. al.* [83], the structure of the design is composed of a band-pass multilayers FSS combined with periodic cylindrical-shaped absorbers. It produced an insertion loss of less than *10 dB* at a frequency of *8 GHz* to *12 GHz. Tsud*a *et. al*. [84] designed a thin wave absorber using a closely placed divided conductive film and resistive film. The proposed design is to be operated at a frequency of *2.5 GHz.*

This present research work has been compared with the existing absorber models and captured in the chapter. 5

2.5 MOSFET Modes and the Principle of Operation

The MOSFET is an insulated gate field effect transistor that is widely used in integrated circuits in electronic devices [85, 86]. It can function as a switching device or amplification device in electronic signal transmission. A MOSFET can be operated in two modes, enhancement mode and depletion mode [87, 88]. Each of these modes is dependent

on the corresponding condition of the MOSFET in ON and OFF state at zero gate-source voltage. Enhancement mode MOSFET is commonly used as a switching element in most integrated circuits. This device is always OFF at zero gate Voltage, they can only be turned on by making the gate voltage higher than the source voltage or making the source voltage higher than the gate voltage. When these two alterations are carried out, two types of enhancement MOSFET are formed the N-MOS or N channel MOSFET and the P-MOS or P channel MOSFET.

To form an N-MOSFET, the gate voltage is made higher than the source voltage, while the P-MOSFET can be formed by making the source voltage higher than the gate voltage when this happens, the threshold voltage will either be positive or negative. The threshold voltage using $V_t = V_G - V_S$. Traditionally, V_t is positive for enhancement N-MOSFET and is negative for enhancement P-MOSFET [24].

Furthermore, most of the research to date has been carried out on n-channel MOS (NMOS) devices, and it was discovered that the carrier mobility of the conventional NMOS transistor is much higher than that of p-channel MOS (PMOS) devices. This is largely due to the fact that the effective mass of electrons is smaller than that of holes. It is, however, not always true for small geometry MOSFET.

2.5.1 Effects of operating conditions on MOSFET characteristics

There has been a rapid in the MOS technology in terms of both propagation speed and integration level. The silicon technology, which is used to fabricate the MOSFET, is today's most mature technology in the semiconductor industry. Due to the advantages in device miniaturization, low power dissipation, and relatively high yield, MOS ICs will continue to dominate the market for some time before another new technology is evolving. The factors that affect the change in physical properties of a MOSFET are studied under two subsections as described below:

A. Temperature

Temperature fluctuations alter threshold voltage, carrier mobility, and saturation velocity of a MOSFET. Temperature fluctuation induced variations in individual device parameters to have unique effects on MOSFET drain current [89]. The absolute values of threshold voltage, carrier mobility, and saturation velocity degrade as the temperature increases. The saturation velocity is typically a weak function of temperature [90, 91].

Threshold voltage degradation with temperature tends to enhance the drain current because of the increase in gate overdrive (V_{GS}-V_t). Alternatively, degradation in carrier mobility tends to lower the drain current. Therefore, an effective variation of MOSFET current is determined by the dominant device parameter variation when the temperature fluctuates [92].

The magnitude of turn-OFF is temperature-dependent and decreases with temperature with a fixed supply voltage, load current, and gate resistance. At the same time, the turn-on increases with increasing temperature. It has been demonstrated by *Liao et. al* [93] that the temperature dependency of variation of drain current results from the positive temperature dependency of the intrinsic carrier concentration and the negative temperature dependency of the effective mobility of the electrons in SiC MOSFET. The temperature dependency is strongly correlated with gate resistance, which varies with different gate resistors. The research results are now beneficial in condition monitoring of power devices, operating temperature, and device reliability.

B. Voltage

The operation of MOSFET under the influence of varying voltage biasing on the gate, drain, and substrate terminals can alter the transistor's electrical characteristics. This is due to the change of the intensity of the electric field acting on the carrier charges. The effect of the body bias on the stability of the threshold voltage of p $^+$ polysilicon gate PMOS transistors stressed in the on-state was investigated by *Atzeni and Manzini* [94]. Special attention was given to PMOS transistors operating at low gate overdrive and non-zero body voltage in their research. A mixed-mode of degradation, including the usual Negative Bias Temperature Instability (NBTI) and the effect of Hot-Hole Injection (HHI) into the gate oxide at high temperature, was reported. The relative importance of both the electric field in the gate oxide and the concentration of cold holes at the interface was pointed out for devices operating in the near-threshold region.

2.5.2 MOSFET regions of operation

The operation of this device happens mainly in three regions as follows**:**

Cut-off region - It is the region where the device will be in the OFF condition, and there zero amount of current flow through it. Here, the device functions as a basic switch and is so employed as when they are necessary to operate as electrical switches.

Saturation region - In this region, the devices will have their drain to source current value as constant without considering the enhancement in the voltage across the drain to source. This happens only once when the voltage across the drain to the source terminal increases more than the pinch-off voltage value. This results in the device functioning as a closed switch where a saturated level of current across the drain to source terminals flows. Due to this, the saturation region is selected when the devices are supposed to perform switching.

Linear/ohmic region - It is the region where the current across the drain to source terminal enhances with the increment in the voltage across the drain to source path. When the MOSFET devices function in this linear region, they perform amplifier functionality.

2.5.3 Application of MOSFET

MOSFET has been used extensively in

- Amplifier design for large frequency applications
- This device can be used as a control for DC motors.
- Chopper amplifiers are perfectly built with MOSFET to provide improved switching rates.
- It works with many electronic elements as a passive component.

Special attention will be given to the N channel MOSFET or NMOS because it forms the basis of this research work. Furthermore, the MOSFET is a symmetrical device, meaning its source and drain can be interchanged with no change in the device performance characteristics. Fig. 2.5 shows an N channel MOSFET or NMOS.
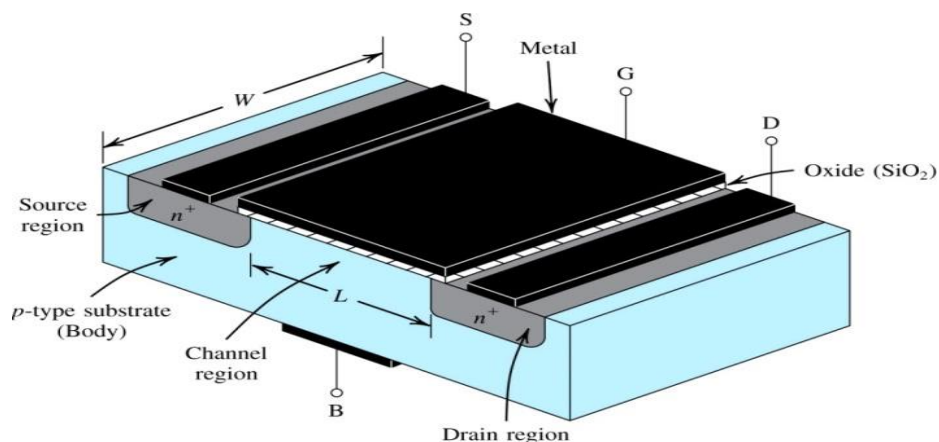
Fig. 2.5.   The physical structure of enhancement type N-MOSFET [24].

Since this work focuses on examining the performance of the proposed model, the performance parameters of previously existing models RF models have been captured in Table.2 to verify the consistency of the model.

Table 2.1 Existing absorber model and performance parameters

Reference	Efficiency (%)	Frequency (GHZ)	Insertion loss (dB)
[75]	> 90	12 – 18	< 10
[76]	--	4 - 13.5	> 10
[77]	--	4.23 – 8.13	< 10
[78]	> 90	9.5 – 55	--
[79]	75	2 – 7	< 10
[80]	94.7	5.9	< 15
[81]	--	2.5 – 5.5	< 10
[82]	--	7.56 - 14.58	< 10
[83]	--	8 – 12	< 10
[84]	90	2 – 5	--

From Table 2.1, it has been observed that parameters such as efficiency, frequency, insertion loss have been used to characterize the performance of the proposed model. These parameters forms the basis of comparison of the proposed model with previously existing models.

2.6 Conclusion

An overview of advantages and potential challenges of wireless technology have been presented. Also, the working principle of the various components of the proposed model construct have been analyzed and a summary of previously existing model and performance parameters for these models have been presented.

Chapter-3

MOSFET BASED ABSORBER OF REFLECTED SIGNAL IN 5G MASSIVE MIMO BASE STATION

3.1 Components Used for the Proposed Model

The main components of the proposed model are basically the four-port circulator and MOSFET. The working principle of each of this device has been explained in chapter 2.2.5
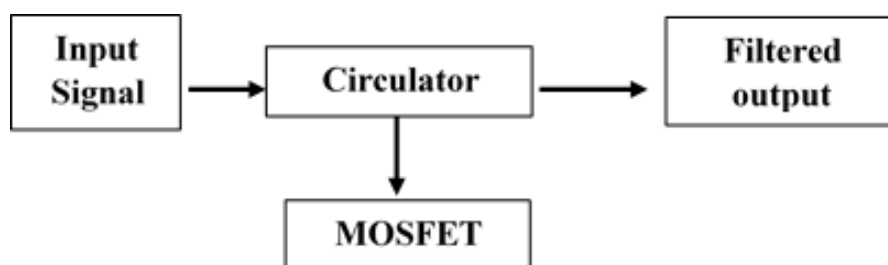
Fig. 3.1.   Process for the design of proposed MOSFET based circulator.

3.1.1 Proposed model (with circulator and port connection to MOSFET in 5G base station)

The proposed design is shown in Fig. 3.2, consist of a four-port circulator, each of these ports (port-1, port-2, port-3, and port-4) are connected to the T_X branch, antenna, R_X branch, and the MOSFET. In this case, the MOSFET is an N-channel enhancement MOSFET, which absorbs the reflected signal from the R_X branch as a result of load mismatch. In the physical layer, the mMIMO technique and high GHz frequency bands are two promising trends for adoption in 5 G technology [95-97]. Millimeter-wave bands such as *28, 38, 64, 71 GHz* were previously considered.

The modulated RF signal from the T_X branch of the base station flows into the circulator via the port-1 of the circulator. The circulator receives this signal and sends it out through its port-2, which has a band-pass filter connected to it. The band-pass filter limits the RF signal to the frequency desired for transmission. Connected to the band-pass filter is a transceiver performing the function of propagating the RF signal into space. The propagated RF signal is received by the transceiver of a neighboring base station. The

signal enters the circulator via the port-2 of the circulator in the neighboring base station. It's outputted through port-3, which has the R_X branch connected to it. Whenever there is a mismatch between the T_X of the transmitting base station and the neighboring base station's R_X branch, some of the signal will be reflected back. The reflected signal from the port-3 of the neighboring base station exits the circulator via its port-4, which has a rectifier and N-channel MOSFET. The rectifier with a filter converts the AC voltage of the reflected signal into DC voltage before it is applied to the drain terminal of the MOSFET for absorption, as shown in Fig. 3.2.
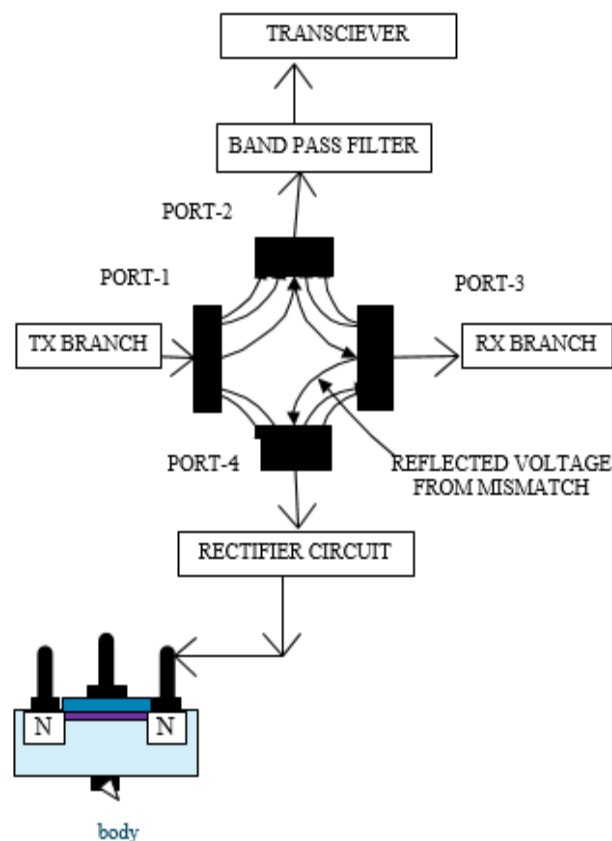
Fig. 3.2. Proposed model of MOSFET based absorber (with the reflected signal in 5G mMIMO base station) [98].

Applying a positive voltage to the gate terminal of the MOSFET creates a channel for the rectified current component of the reflected signal to flow from the drain terminal to the source terminal of the MOSFET [24, 95, 96]. The current is measured at the source terminal to determine the level of reflection, which is the main objective of this work absorb. A zero current at the source terminal of the MOSFET signifies zero reflection from

the R$_X$ branch. A greater than zero current at the source terminal signifies reflection from the R$_X$ branch, and it has been absorbed by the MOSFET. This current can be observed/measured by an ammeter.

1.2 Parametric analysis and its discussion

Performance or sensitivity analysis of the proposed model will not be complete without a study of the influence of different physical parameter on the solution to the problem. Some of these physical parameters are related in teems of frequency, power, resistance, current and voltage. These physical parameters have a negative or positive effect on the overall performance of the proposed model circuit and therefore needs to be analysed.

In this research work, the *28 GHz* band have been considered for which the base station transmission power is *43 dBm* (equivalent to *20 W* peak power) for a *50 Ω* resistance system using $P_{dBm} = 10\log\left(P_{mw(50\Omega)}\right)$ to calculate peak voltage the used expression is [104,105 107, 108]:

$$P_{dBm} = 10\log\left(P_{mw(50\Omega)}\right) \tag{3.1}$$

$$P_{dBm} = 43 \ dBm$$

Substituting $P_{dBm} = 43 \ dBm$ into Eq. (3.1):

$$10\log\left(P_{mw(50\Omega)}\right) = 43,$$

Then, $P_{mw(50\Omega)} = 19952.6$, Converting to watt, $P_{w(50\Omega)} = 19.95 \ W$, will give $P_{Peak} = 20 \ W$.

The peak voltage V_{peak} is given as:

$$P_{mw(50\Omega)} = \frac{1}{R}\left(\frac{V_{peak}}{\sqrt{2}}\right)^2 \times 1000 \tag{3.2}$$

$$19952.6 = \frac{1}{50}\left(\frac{V_{Peak}}{\sqrt{2}}\right) \times 1000$$

Therefore, $V_{peak} = 44.67$, means for power *20 W*, the received V_{peak} is *44.67 V*.

To calculate the peak current, the used expression is :

$$P_{peak} = I_{peak} V_{peak} \qquad (3.3)$$

Here $I_{peak} = 0.447\ A\ or\ 447\ mA$. From this analysis, the peak transmission power, voltages, and current in the T_X branch of a *28 GHz* band 5 G base station are *20 W, 44.67 V,* and *0.447 A*, respectively.

The RF signals are alternating in nature, so all values of voltage, current, and power are AC values. When this signal is received at the R_X branch connected to the circulator, not all the signals are absorbed by the R_X circuit. Some of them are reflected back due to mismatch, creating a high VSWR, causing the signal to be reflected. Since the circulator is a non-reciprocal device, the reflected signal will go out through the port-4 of the circulator into the rectifier circuit, converting the AC power, voltages, and current into its DC equivalent before it is applied to the N-channel enhancement MOSFET as shown in Fig. 3.2.

Assuming the reflected signal power is *19 dBm*, applying the formula for peak power, voltages, and current will be able to get the peak power *0.079 W*, peak voltages *2.7 V,* and peak current *29 mA*. Since the reflected signal is coming out of port-3, the R_X branch, the signal goes out through port-4 of the circulator where the N-channel MOSFET is connected. Therefore, since these values are AC, they are rectified to DC values by a rectifier connected between port-4 and the MOSFET.

The DC components of voltage and current given by [105]

$$V_{DC} = \frac{V_{peak}}{\sqrt{2}} \qquad (3.4)$$

Substitute V_{peak} = 2.7V, into V_{DC}, Now, V_{DC} is *1.86 Volts*, where:

$$I_{DC} = I_{peak} / \sqrt{2} \qquad (3.5)$$

Therefore, I_{DC} is *0.02 mA* where I_{DC} is the drain current I_D, and V_{DC} is the drain to source voltage V_{DS} . Now V_{DS} and I_D are *1.86 Volts* and *20 mA*, respectively. These are the Expected values of voltage and currents after rectification that will be applied to the drain terminal of the N-channel MOSFET.

For drain current I_D to flow from drain to source, a channel must be created between the drain and the source. A positive voltage is applied to the MOSFET gate terminal, and the source terminal is grounded to form this channel. The maximum allowable gate terminal voltage for most MOSFET is $\pm$ *20 V* applying a voltage higher than this will damage the MOSFET. This maximum allowable voltage is set at the MOSFET design stage. In this case, *9.5V* has been used for further design.

After grounding the source terminal and applying a positive voltage of *9.5 V* to the gate terminal, the gate voltage appears between the gate and the source (V_{GS}). As soon as V_{GS} is applied, the free holes underneath the gate are repelled further down to the base of the substrate leaving behind a career depletion region. Electrons from both the drain and source regions are attracted to the base of the gate terminal. When a sufficient number of electrons accumulate in the carrier depletion region, a channel is formed connecting the drain and the source n^+ regions. The channel formed in this case is called N-channel or inversion layer. As soon as this channel is created between the source and the drain regions, the current I_D carried by mobile electron flows through the induced N-channel region.

After creating a channel for the flow of current I_D from drain to source, the circulator's rectified voltage is applied to the drain terminal, and the current I_D flows from drain to source. Along the channel, from drain to source, V_{DS} value decreases because of the channel's resistance. This value will be measured with the use of a voltmeter at the source terminal of the MOSFET. In addition, the value of current I_S at the source terminal can be measured by using an ammeter and can be calculated theoretically by [24, 26,]:

$$I_S = Ch\arg e \ per \ unit \ channel \ length \ \times \ Electron \ drift \ velocity$$

$$I_S = \frac{Q}{L} \times Electron \ drift \ velocity \tag{3.6}$$

where charge per unit length is given as:

$$Q = C_{ox}WLV_{ov} \tag{3.7}$$

Given that:

$$C_{ox} = \varepsilon_{ox} / t_{ox} \tag{3.8}$$

where $\varepsilon_{ox} = 3.9\varepsilon_O$ and $\varepsilon_O = 8.85 \times 10 - 12 f / m$, where L, W, and t_{ox} are channel length,

channel width, and thickness of the Silicon oxide, respectively. The ε_{ox} and ε_O are the permittivity of silicon dioxide and permittivity constant respectively, and C_{OX} is the capacitance of Silicon oxide. Electron drift velocity is given by [24]:

$$Electron\,drift\,velocity = Electric\,field \,\times\, Electron\,mobility$$

$$Electron\,drift\,velocity = |E| \,\times\, \mu_n \qquad (3.9)$$

Where μ_n is electron mobility of N channel MOSFET.

$Electric\,field\,E\,is\,given\,as$:

$$|E| = \frac{V_{DS}}{L}$$

(3.10)

Substitute Eq. (3.10) into Eq. (3.9)

$$Electron\,drift\,velocity = \left(V_{DS}\,/\,L\right) \,\times\, \mu_n \qquad (3.11)$$

Substitute Eq. (3.7) and Eq. (3.11) into Eq. (3.6); Recall Eq. (3.6):

$$I_S = \frac{Q}{L} \times Electron\,drift\,velocity$$

$$I_S = \left(\frac{C_{ox}WLV_{ov}}{L}\right) \times \frac{V_{DS}}{L} \times \mu_n$$

$$I_S = C_{ox}WV_{ov} \times \frac{V_{DS}}{L} \times \mu_n$$

$$I_S = \left[\mu_n C_{ox}\left(\frac{W}{L}\right)V_{ov}\right]V_{DS} \qquad (3.12)$$

V_{OV} is given as:

$$V_{ov} = V_{GS} - V_t \qquad (3.13)$$

Substitute Eq. (10) into Eq. (9):

$$I_S = \left[\mu_n C_{ox}\left(\frac{W}{L}\right)V_{ov}\right]V_{DS}$$

31

$$I_S = \left[\mu_n C_{ox} \left(\frac{W}{L} \right) V_{GS} - V_t \right] V_{DS} \tag{3.14}$$

The current I_S at the source terminal of the N-channel MOSFET connected to port-4 of the circulator can be calculated using Eq. (3.14). In addition, as current travel along the channel from drain to source, there is a voltage drop along the channel from drain to source region. This voltage drop is a result of the channel resistance (R_{DS}), which can be calculated by [24, 26, 88]:

$$V = IR$$
$$V_{DS} = I_S R_{DS} \tag{3.15}$$

Substitute Eq. (3.14) into Eq. (3.15):

$$V_{DS} = \left[\mu_n C_{ox} \left(\frac{W}{L} \right) V_{GS} - V_t \right] V_{DS} R_{DS}$$

$$\frac{V_{DS}}{\left[\mu_n C_{ox} \left(\frac{W}{L} \right) V_{GS} - V_t \right] V_{DS}} = R_{DS}$$

$$R_{DS} = 1 / \left[\mu_n C_{ox} \left(\frac{W}{L} \right) V_{GS} - V_t \right]$$

The channel resistance R_{DS} can be calculated using the formula:

$$R_{DS} = \frac{1}{\left[\mu_n C_{ox} \left(\frac{W}{L} \right) V_{GS} - V_t \right]} \tag{3.16}$$

where the device designer can select w and L to give the *V-I* characteristics desired for the given fabrication process. To calculate the channel conductance G_{DS}, use the formula

$$G_{DS} = 1/R_{DS}$$

$$G_{DS} = \mu_n C_{ox} \left(\frac{W}{L}\right) V_{GS} - V_t \qquad (3.17)$$

where:

$$Aspect\ ratio = \left(\frac{W}{L}\right)$$

$$K_n^I = \mu_n C_{ox} \qquad (3.18)$$

Kn^1 Is the process Trans conductance parameter, and the subscript n shows that it is an n channel MOSFET. Transconductance parameter K_n of the N channel MOSFET use the formula:

$$K_n = \ Process\ transconduc\tan ce\ parameter \times Aspect\ ration$$

$$K_n = \mu_n C_{ox} \left(\frac{W}{L}\right) \qquad (3.19)$$

The source current I_S can be calculated or measured with the use of an ammeter. Finally, the current I_S at the source terminal is less than or equal to the sum of the current I_D at the drain terminal and the gate current I_G, which is 0, therefore:

$$I_S \leq I_D + I_G$$

$$I_S \leq I_D + 0$$

$$I_S \leq I_D \qquad (3.20)$$

The current at the source terminal for a small value of V_{DS} is given as:

$$I_S = \left[\mu_n C_{ox} \left(\frac{W}{L}\right) V_{GS} - V_t\right] V_{DS}$$

Now, Eq. (3.20) becomes:

$$\left[\mu_n C_{ox} \left(\frac{W}{L} \right) V_{GS} - V_t \right] V_{DS} \leq I_D \qquad (3.21)$$

Since the reflected signal from the port-4 of the circulator is rectified to produce a drain current I_D of *20 mA* at *1.86 V* drain to source voltage (V_{DS}), this drain current value will be greater than or equal to the current I_S at the source terminal when measured with an ammeter because of the resistance of the channel. Recall $I_D = 20\ mA$, therefore, using Eq. (3.20), it can be calculated that $I_S \leq 20\ mA$.
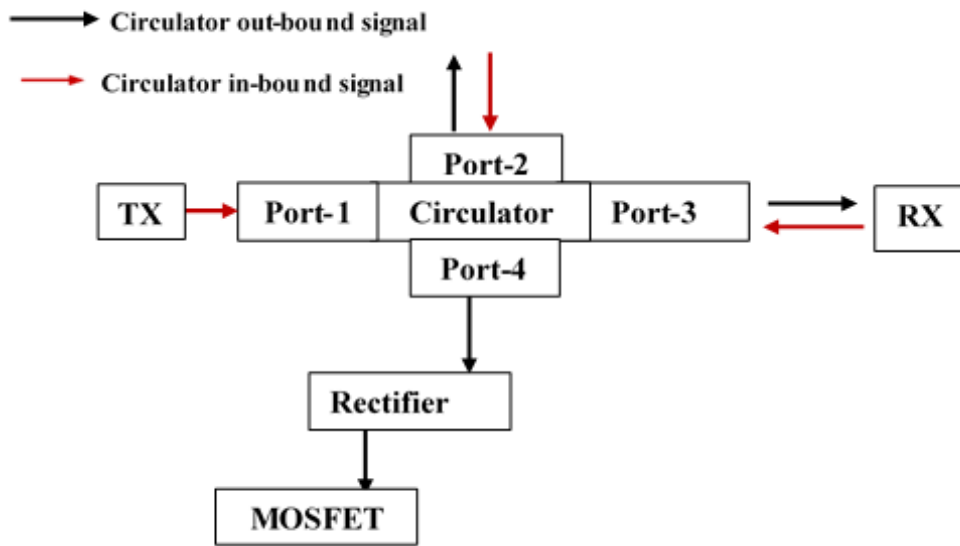
Fig. 3.3. MOSFET and circulator port connection.

In the case where the reflection from port-3 of the circulator is small, the value of V_{DS} is also small, the MOSFET behaves as linear resistance R_{DS} above whose value is controlled by the gate voltage V_{GS}. The characteristics curve of the current I_S and voltage V_{DS} when the reflection from port-3 is small, resulting in a small value of V_{DS} as shown [24]. Due to $I_S \leq I_D$, the reflected signal coming out from port-3 is possible to enter into port-4 to increase and become large. At this condition, V_{DS} values will increase at the same rate as the reflected signal because the reflected signal varies directly as V_{DS}. In this case, the resulting characteristic curve of current I_S, and voltage V_{DS} at the source terminal of the N-channel MOSFET is not the same.

This change in the characteristic curve of current I_S, and voltage V_{DS} is a result of the increase in the channel resistance because as voltage increases, hence the resistance

increases. In addition to this, another characteristic of the MOSFET that changes are the overdrive voltage. This MOSFET characteristics changes from V_{OV} to a value that is dependent on the average value of V_{DS} along the channel:

$$V_{ov} = V_{ov} - \frac{V_{DS}}{2} \tag{3.22}$$

Furthermore, an increase in reflection causes the channel to become more tapered, and the current I_S at the source terminal can be represented as [24]:

$$I_S = \left[\mu_n C_{ox} \left(\frac{W}{L} \right) \left(V_{ov} - \frac{V_{DS}}{2} \right) \right] V_{DS} \leq I_D \tag{3.23}$$

As stated earlier, it is not feasible for a transmission system to be lossless, and the 5 G mMIMO base station is not an exception to this fact. Reflection is bound to occur whenever there is a mismatch between the base station's T_X branch and R_x branch. When the reflection is coming out from the port-4 of the circulator, it is not applied directly to the MOSFET drain terminal because it is alternating in nature, so it needs to be rectified before it is fed into the MOSFET drain terminal. From the analysis of the proposed model, the reflection is bound to occur under two conditions:

A. When the reflection from port-3 of the circulator is small and almost constant, resulting in a small and almost constant value of V_{DS}, hence:

$$I_S = \left[\mu_n C_{ox} \left(\frac{W}{L} \right) V_{GS} - V_t \right] V_{DS} \leq I_D \tag{3.24}$$

Since V_{DS} value is kept small, it behaves like a linear resistance whose value is controlled by V_{GS}. The characteristics curve of the current I_S, and voltage V_{DS} is captured in various literatures [24].

B. When the reflection from port-3 of the circulator is increasing, increasing the value of V_{DS}:

$$I_S = \left[\mu_n C_{ox} \left(\frac{W}{L} \right) \left(V_{ov} - \frac{V_{DS}}{2} \right) \right] V_{DS} \leq I_D \tag{3.25}$$

where I_D is *20 mA*. Since the value of I_S is a function of the channel resistance (as in Eq. (3.15)), getting the true value of I_S allows comparison to check if truly $I_S \leq I_D$ as stated in the proposed model analysis.

This proposed model is modest in its structure, implementation, and low power consumption of the MOSFET.

3.3 Conclusion

Interference caused by signal reflections from a circulator in the 5G base station (for unmatched termination between the T_X branch and R_X branch) has been analysed. The proposed model has theoretically proved that destructive interference caused by reflection from the R_X branch can be avoided by using MOSFET technology to absorb the signal. Also, various current and voltage relationship of the reflected signal has been established for the proposed model.

Chapter-4

SIMULATION ANALYSIS OF MOSFET BASED ABSORBER FOR REFLECTED RF SIGNAL IN 5G MASSIVE-MIMO BASE STATION

4.1 Basics of RF Rectification Process

A four-port circulator connects the T_X branch, R_X branch, and antenna branch, the function of the circulator is to route radio frequency signal between all branches connected to it [95-97]. It is non-reciprocal (behaviour in one direction is different from their behaviour in another direction). Power is transferred from one port to the adjacent port in a prescribed order. It is also a device used for transmission in which microwave or radio-frequency signal entering any port are passed on to the next port in rotation. A port in this context is the point where an external waveguide or transmission line is connected to the device [97].

4.2. Circulator Basics and Advancements

A novel three-port active circulator was proposed by *Moussa et. al.* [99]. This circulator was composed of a phase divider with one transistor and a special form of Wilkinson power splitter operating as a power combiner. An active quasi-circulator at *30 GHz* was designed and fabricated by *Chang et. al.* [100] at TSMC *0.18-μm* mixed-signal CMOS technology. The current reuse technique was integrated with a common source stage to form the quasi-circulator core with reduced power consumption. A three-port active circulator and active quasi-circulator based on the bridged-T network were designed and fabricated by *Wang et. al.* [17] at standard *0.18-μm* CMOS technology. An active quasi-circulator MMIC was designed and fabricated by *Shin et. al.* [18] at standard *0.18-μm* CMOS technology. It combines the common source, common gate, and common drain configurations to improve the isolation between ports and improved insertion loss.

The circulator can be used as an isolator/duplexer or perform both operations in a transmission system [42, 43, 101]. In a four-port circulator, the signal entering by port-1 exits the circulator via port-2, the signal entering by port-2 exits the circulator via port-3,

the signal entering through port-3 exits the circulator via port-4. Lastly, the signal entering the circulator via port-4 exits the circulator via port-1, as captured in chapter 2.2.5. Fig 4.1 shows the port connection of a basic circulator.
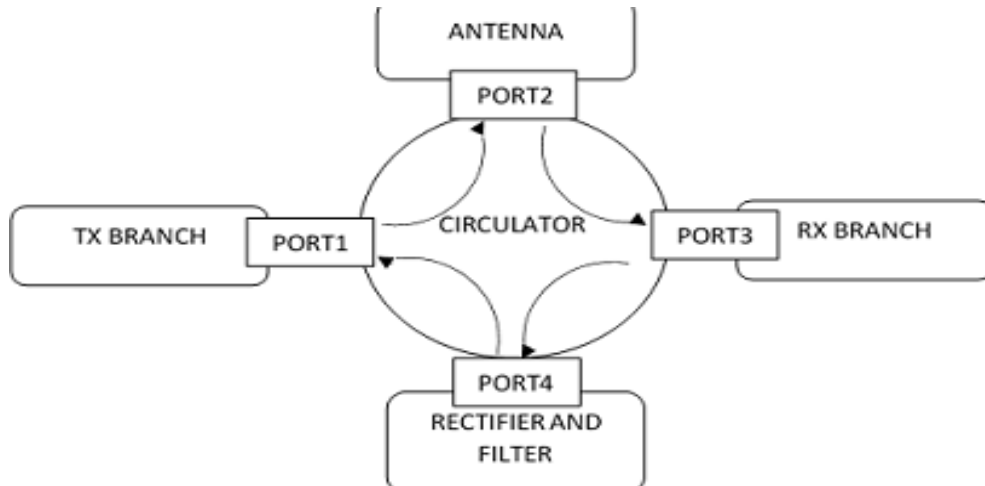
Fig 4.1.   The basic model of RF pre-rectification.

The modulated RF signal from the T_X branch of the base station flows into the circulator via the port-1 of the circulator. The circulator receives this signal and sends it out through its port-2, which has a band-pass filter connected to it. The band-pass filter limits the RF signal to the frequency desired for transmission. Connected to the band-pass filter is a transceiver that performs the function of propagating the RF signal into space. The propagated RF signal is received by the transceiver of a neighbouring base station. The signal enters into the circulator via the port-2 of the circulator in the neighbouring base station. It is outputted through port-3 has the R_X branch connected to it. Whenever there is a mismatch between the T_X of the transmitting base station and the neighbouring base station's R_X branch, some of the signal will be reflected back. The reflected signal from the port-3 of the neighbouring base station exits the circulator via its port-4, which has a rectifier connected to it. As stated in chapter 1.3, Models for simulation were insufficient to provide real ports, for this reason, a sinusoidal voltage source has been used to provide an equivalent source or T_X branch terminal voltage component of Incident RF power. With the help of a voltage divider, the voltage component of reflected RF power from the R_X branch connected to the circulator was generated and applied to the rectifier's input terminal in the proposed model.

$$V_{out} = V_{in}\left[\frac{R_2}{R_1 + R_2}\right]$$

(4.1)

where V_{in} is Source or T_X branch terminal voltage component of Incident RF power and V_{out} is voltage component of reflected RF power from R_X branch. The values of resistors R_1 and R_2 required to produce a voltage drop equivalent to the voltage component of the reflected RF power from the R_X branch have been generated with online software.

Considering *19 dBm* reflection loss from the R_X branch of the base station, the values of resistors R_1 and R_2 required to produce a voltage drop equivalent to the voltage component of reflected RF power have been calculated to be 108.95 Ω and 1700 Ω, respectively. Substituting these values of R_1, R_2, and V_{in} into Eq. (4.1). Recall,

$$V_{out} = V_{in}\left[\frac{R_2}{R_1 + R_{n2}}\right]$$

where $V_{in} = 44.662\ Volts$, therefore, $V_{out} = 2.69\ V$.

Similar calculations have been carried out for three other reflection cases from the R_X branch connected to the circulator. The equivalent resistor values needed to produce the required output voltage recorded in Table. 4.1. However, these values of power for the chosen may be high, they have been used to accurately predict and evaluate the model.

Table 4.1 Values for resistors needed to produce the required voltage output

Reflected RF power P(dBm)	V_{in} (volts)	V_{out} (volts)	R_1 (Ω)	R_2 (Ω)
3	44.67	0.45	1700	17.19
5	44.67	0.56	1700	21.82
13	44.67	1.44	1700	56.64
19	44.67	2.69	1700	108.95

4.3 Rectification of Reflected RF Signal

The 5G base station's ultimate goal is the efficiency of various components used for its construct. For this reason, a full-wave rectifier was used in place of a halfway rectifier as it produces twice the efficiency of a half-wave rectifier. Though, the use of two additional diodes for the rectifier construct is a disadvantage because each of the diodes causes a voltage drop, thus reducing the voltage at the output terminal of the rectifier

[18,19,102-105]. However, considering the conditions for MOSFET absorption and the working of the MOSFET voltage drop is not a major concern in this research and has a minimal effect on the overall research conclusion.

Putting all these into consideration, a voltage source representing the reflected radio frequency power from the port-4 of the circulator is applied to the input terminal of the rectifier, and a combination of *2 KΩ* load resistor and the four-diode combination carries out the rectification process taking into consideration the on and off states of the diodes and the potentials at each node of the rectifier as shown in Fig. 2. During the positive half cycle, diode D_3 and diode D_4 are in ON state, for the negative half cycle, diode D_1 and diode D_2 are in ON state, and the type of wave present at the output of the rectifier, in this case, is a pulsating as shown in Fig. 4.4 (a) and (b).
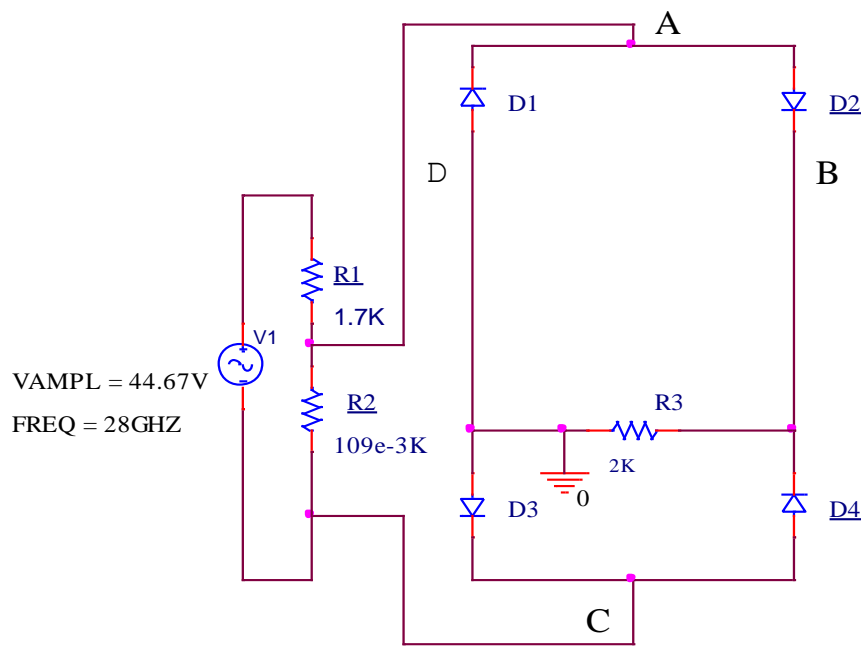
Fig 4.2 Basics of rectification of reflected RF signal.

In the rectifier configuration (Fig. 4.2), the diodes keep switching connections to the resistor through the various available nodes so that current flows in only one direction through the resistor. The resistor can be replaced with any other circuit, including more power supply circuitry (such as the LC filter), and still realize the same behaviour from the bridge rectifier as explained in further sections.

4.4 Filtration of Pulsating DC Signal with the Designed MOSFET Based Absorber

For a MOSFET device to function properly, it is important to apply a pure and consistent DC signal to the MOSFET drain terminal, as the signal from the output of the rectifier connected to the circulator is pulsating [18,19,105]. In Fig. 4.6, to achieve a pure DC, a capacitor and an inductor have been connected in parallel and series, respectively, with a load resistor [106, 107]. This capacitor filters the variation in voltages at the rectifier's output, while the inductor filters the variation in current. Without the capacitor, a pulsating DC signal will exist, but the variation will be lesser with the capacitor and inductor.

When the voltage is rising, the capacitor stores the charge (charging mode), absorbing energy from the circuit. When the voltage across the load resistor decreases, the capacitor releases its stored energy into the circuit, thus preventing the voltage from dropping so low. When the voltage rises again, the capacitor absorbs the circuit's energy, thus preventing the voltage from rising too quickly. The capacitor absorbing and releasing energy to the circuit causes the voltage to be more consistent rather than falling quickly and then rising quickly. It smoothens out the pulsating DC signal.

The variation in voltages after filtering is called a ripple voltage. Reduction in the ripple voltage is achieved by increasing the capacitor value's value or increasing the load resistor that may not always have control over [106-109]. In addition to this, capacitance selection is an important issue in the circuit, even though it is a very effective way of reducing the ripple voltage, it also has a problem.

The inductor has the same effect as the capacitor, but when the current goes up, the inductor will oppose the current increase. It does so by absorbing energy and storing it in its expanding magnetic field. When the current goes down, the inductor's magnetic field releases its stored energy back to the circuit, thus supporting the falling currents.

4.5 Simulation Analysis of the Designed Circuit

The simulator used for the proposed model design is the PSPICE circuit analysis tool used for extracting key voltages and currents. Information can be entered into the PSPICE software by designing a visual a schematic of the any model. By running the design, the simulator transforms the design into a nested list. The PSpice is a full featured

analog circuit simulator with support for digital elements. It integrates easily with Cadence Printed Circuit (PCB) schematic entry solutions like OrCAD Capture and comes with an easy-to-use graphical user interface.

For simulation, a sinusoidal voltage source has been used to provide the equivalent reflected power from the base station's R$_X$ branch. The frequency of the voltage source was set to *28 GH*z. However, at 5G frequencies, voltages and current concepts become difficult to relate with during simulation. Also, when frequencies are too high, it becomes difficult for discrete capacitors and inductors to be practical. A combination of Schottky diode and distributed circuit will be employed for the rectification and filtration process during the proposed model's physical implementation at 5G frequency.

4.5.1 Simulation analysis for the basic model

The basic circuit (Fig. 4.2) has been simulated, and the equivalent values of peak voltages and currents have been deduced from the input plots. Parameters such as root mean square value of voltage, current, and peak power have been calculated from the resulting values of peak voltages at the rectifier's input terminal. The generated waveform usually has a voltage or current plot against time. The horizontal axis shows the passing of time, progressing from left to right. The vertical axis shows the quantity measured, which in this case, voltage or current. Fig 4.3 a and b shows the waveforms of voltages and current at the input of the rectifier circuit of Fig. 4.2.

Fig 4.4 shows the waveforms of pulsed values for voltages and current at the output of the rectifier circuit of Fig. 4.2. From the pulsed values of various voltages and currents deduced from the rectifier's output plot, parameters such as ripple factor expected DC current have been calculated and recorded. In addition to this, the rectifier's output plot has a combination of AC and DC characteristics, which is not ideal for MOSFET's proper functioning.
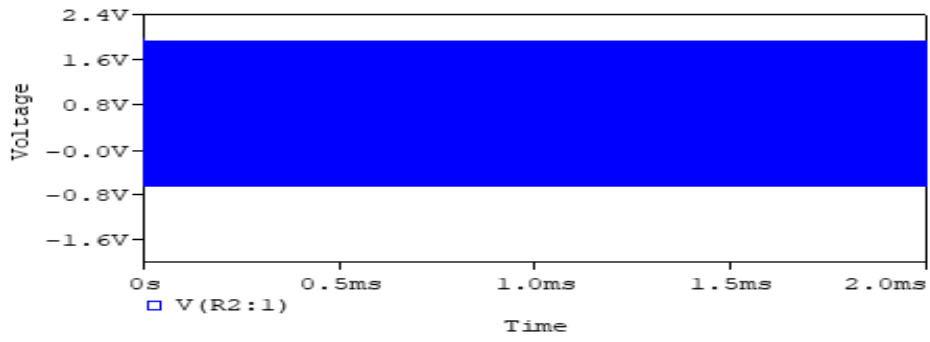
(a)
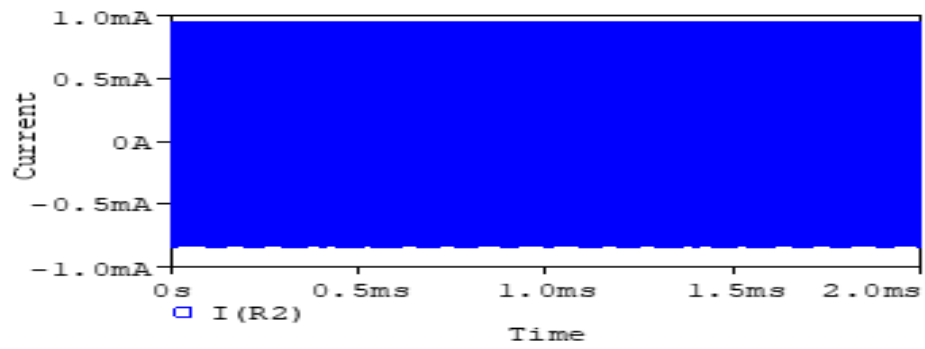
(b)

Fig. 4.3 Plot for rectifier input (a) voltage, and (b) current.
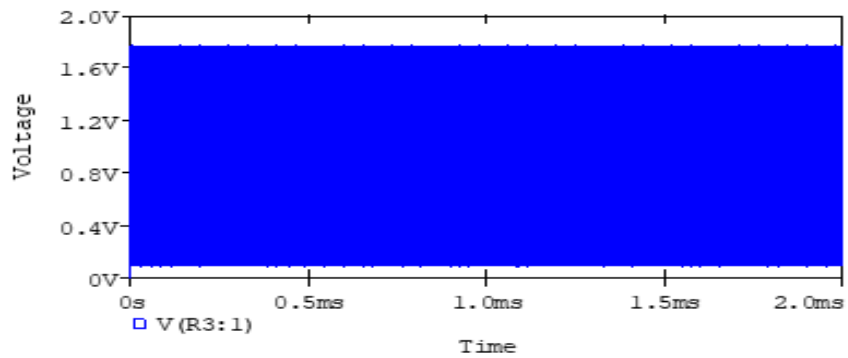
(a)
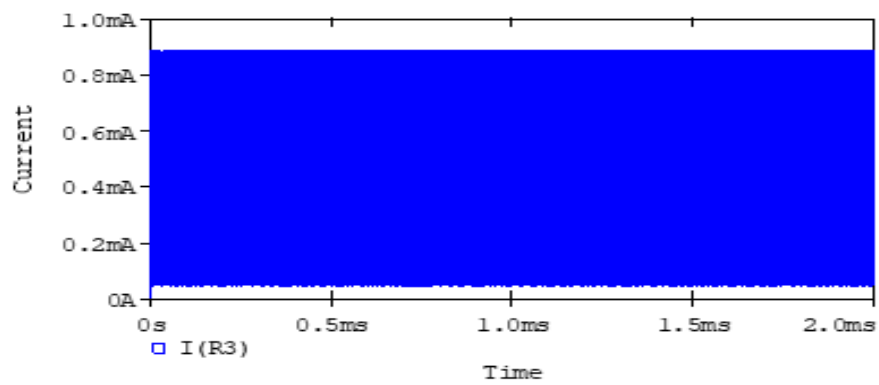
(b)

Fig. 4.4. Plot for rectifier output (a) voltage and (b) current.

Power supply with very low noise and DC ripple is required for MOSFET. For this reason, the output of the rectifier must be filtered using highly efficient filters. In the simulation, an LC filter has been used. To achieve a smooth output, the values of capacitors and inductors have been calculated from the values of voltages and currents deduced from the plots of waveforms, as shown in Fig. 4.4. From the plots, the peak values of voltages and currents are *1.8 V* and *0.9 mA*, respectively. The values of different parameters needed to calculate the rating of capacitor and inductor used for the filter design have been determined from these values.

However, on the physical implementation of the proposed model, the values of the capacitor, inductor, and resistor in the rectifier circuit will be tuned to meet the frequency requirement of the 5G base station, in addition to this, the proposed model is largely dependent on the frequency at which the rectifier circuit is designed.

$$V_{rms} = V_{peak} \times 0.707 \tag{4.2}$$

Since V_{peak} and I_{peak} have been generated from plot as, *1.8 Volts* and *0.9 mA* respectively, now: V_{rms} is *1.28 Volts*, hence,

$$V_{DC} = \frac{2V_{peak}}{\pi} \tag{4.3}$$

For a peak voltage of *1.8 V*, V_{DC} is *1.446 V*

$$I_{rms} = 0.707 \times I_{peak} \tag{4.4}$$

$$I_{DC} = \frac{2I_{peak}}{\pi} \tag{4.5}$$

For a peak current of *0.9 mA*, using Eq. (4.4) and Eq. (4.5), I_{rms} and I_{DC} has been calculated *as 0.64 mA* and 0.57 *mA*, respectively. The load resistance (R_L) is given by [104].

$$R_L = \frac{V_m}{I_m} \tag{4.6}$$

Since V_m and I_m is equal to V_{peak} and I_{peak} respectively, now $R_L = 2\ K\Omega$. The values of capacitor and inductor needed for LC filter design is dependent on the ripple factor, where ripple factor is given by [107].

$$RippleFactor = \frac{\sqrt{I_{rms}^2 - I_{DC}^2}}{I_{DC}} \tag{4.7}$$

Now substitute values of I_{rms} and I_{DC} into Eq. (4.7). Since I_{rms} and I_{DC} are equal to *0.64 mA* and *0.57 mA*, the Ripple factor becomes *0.333*. Also, the impedance of the inductor used for the design, is given by [107].

$$X_L = \frac{V_{peak}}{I_{rms}}$$

(4.8)

Therefore, at a peak voltage of *1.8 V*, and *0.64 mA* rms value of current, the equivalent value of X_L is *3 KΩ*. The inductance can be calculated using:

$$X_L = 2\pi fL \tag{4.9}$$

where *f* is the frequency of the sinusoidal voltage source, which has been chosen to be *28 GHz*. Substituting values of the X_L and f into Eq. (4.9), L is calculated as 0.017×10^{-6} H. where impedance of the capacitor is calculated as :

$$RippleFactor = \frac{X_{C_1} \times X_{C_2} \sqrt{2}}{3X_L}$$

(4.10)

But $X_{C1} = X_{C2} = X_C$, Now ripple factor is calculated as :

$$RippleFactor = \frac{X_C^2 \sqrt{2}}{3X_L}$$

Substitute values of X_L and ripple factor into Eq. (4.10), $X_c = 46.05\ \Omega$. To achieve maximum filtering, the inductor's impedance must be higher than the capacitor's impedance. To calculate the value of capacitor C use :

$$C = \frac{1}{2\pi f X_C}$$
(4.11)

Substitute values of f and X_C into Eq. (4.11). Fig. 4.5 (a) and (b) show the resulting plots for pure voltage and current, respectively.

The voltages and current values at the drain and source terminal have been deduced after performing a transient analysis using the p-spice software from these output plots. However, values may not be exact, but errors from plots are insignificant. From the plots, it can be deduced that $V_{DC} = 1.6\ V$ and $I_{DC} = 0.4\ mA$.
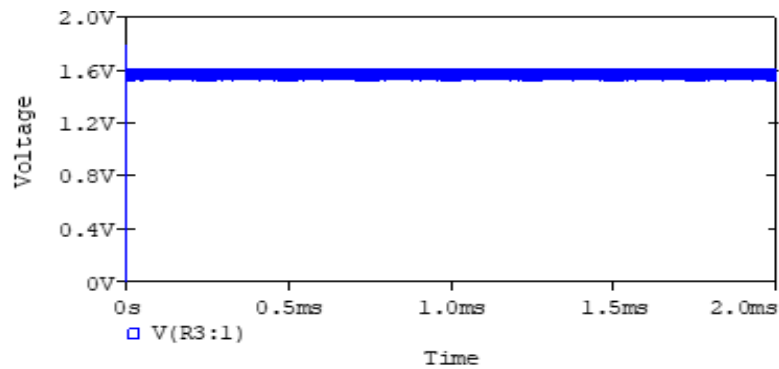
(a)
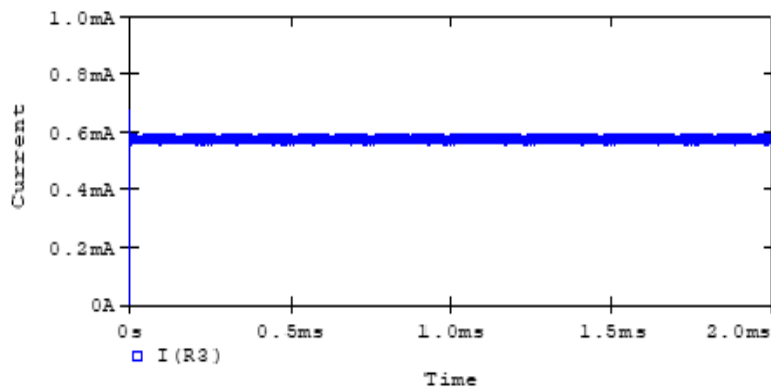
(b)

Fig. 4.5. Plot for rectifier filtered output (a) voltage, and (b) current.

4.5.2 Simulation analysis of designed circuit (MOSFET based absorber)

In this simulation analysis, four reflection cases (*19 dBm,13 dBm,5 dBm,* and *3 dBm* reflection loss) from port-3 of the circulator have been examined to determine the consistency of various parameters used in the proposed model construct [110-112]. At these conditions, the values of V_{DS} increases at the same rate as the reflected signal because the reflected signal varies directly as V_{DS}. Where reflected power can be calculated using:

$$P = \frac{1}{R}\left(\frac{V_{peak}}{\sqrt{2}}\right)^2 \tag{4.12}$$

Using Eq. (4.12) and formulas in previous sections, the input values of voltages and currents of the rectifier have been calculated at different condition of reflection from port-4 of the circulator and recorded in Table 4.2. At the rectifier's output terminal, the values of peak voltages and currents are pulsating, as shown in Fig. 4.4 a and b. From the simulation experiment, these values were deduced from the output plot, and its equivalent RMS value generated and recorded in Table 4.3.

Table 4.2.   Rectifier input terminal parameters

Reflected RF power P(*dBm*)	Reflected RF power P(*watt*)	V_{peak} (*volts*)	V_{rms} (*volts*)	I_{peak} (*mA*)	I_{rms} (*mA*)
3	0.000004	0.447	0.316	0.009	0.007
5	0.0000151	0.56	0.4	0.027	0.023
13	0.0002448	1.44	1.0	0.17	0.15
19	0.00359	2.7	1.9	1.33	0.566

Table 4.3.   Rectifier output terminal parameters

Reflected RF power P(*dBm*)	V_{peak} (*volts*)	V_{rms} (*volts*)	I_{peak} (*mA*)	I_{DC} (*mA*) Expected	I_{rms} (*mA*)	ripple factor
3	0.0038	0.002	0.0019	0.0012	0.00 13	0.42
5	0.0097	0.0068	0.00485	0.0031	0.0034	0.45
13	0.56	0.396	0.27	0. 179	0.19	0.353
19	1.8	1.27	0.9	0.57	0.64	0.333

From the plots, the peak values and RMS values of current at the input and output terminal of the rectifier have been observed to be different. However, for a MOSFET to function effectively, the values of applied current and voltages must be pure rather than pulsating. To generate a pulsating DC, the rectifier's output must be filtered as explained in Section 4.1.4 [106, 107]. Using the formulas in section 4.2.1, the value of capacitance (C) and inductance (L) has been calculated and recorded, as shown in Table 4.4.

Table 4.4.   Filter design parameters

Reflected RF power (dBm)	L (H)	C (uF)
3	16.6×10^{-9}	111.3×10^{-10}
5	16.2×10^{-9}	108.9×10^{-10}
13	16.75×10^{-9}	121×10^{-10}
19	17×10^{-9}	123×10^{-10}

With the values of parameters in Table 4.1 and Table 4.4, the proposed model's equivalent circuit has been designed using the P-spice software, as shown in Fig. 4.6. To simulate the proposed model, the threshold voltage of the MOSFET was set to *0.8 V*, and the gate voltage was gradually increased until the MOSFET was fully ON at *9.5 V*. After running the simulation, the value of current and voltage at the source and drain terminal of the MOSFET were measured at different reflection condition from port-4 to verify the correctness of the relationship for MOSFET [24].

$$I_S = \left[\mu_n C_{ox} \left(\frac{W}{L} \right) V_{GS} - V_t \right] V_{DS} \leq I_D \qquad (4.13)$$

The purpose of this research is targeted towards using a MOSFET to absorb reflected RF power in 5G base station the relationship $I_S \leq I_D$ and $V_{DS} = 0$ at the source terminal of the MOSFET must be consistent for all cases of reflection from port-4 of the circulator. Fig. 4.7 and Fig. 4.8 show the voltages' plots and current at the drain and source terminal of MOSFET, under *19 dBm* reflection from port-4 of the circulator. There is a voltage drop

from *1.6 V* to *0 V* ,because of MOSFET's channel resistance. The channel resistance is given by [24]:

$$R_{DS} = \frac{1}{\left[\mu_n C_{ox} \left(\frac{W}{L} \right) V_{GS} - V_t \right]}$$

(4.14)
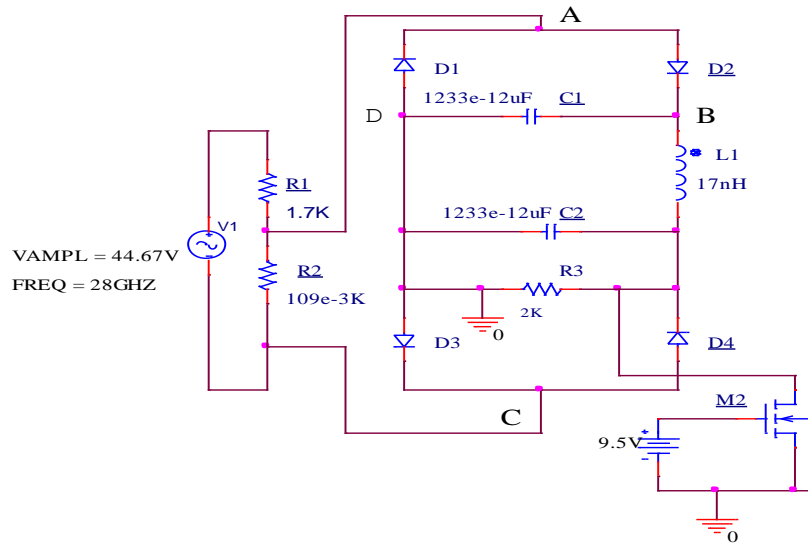
Fig. 4.6.   Circuit for MOSFET based absorber of reflected RF signal.
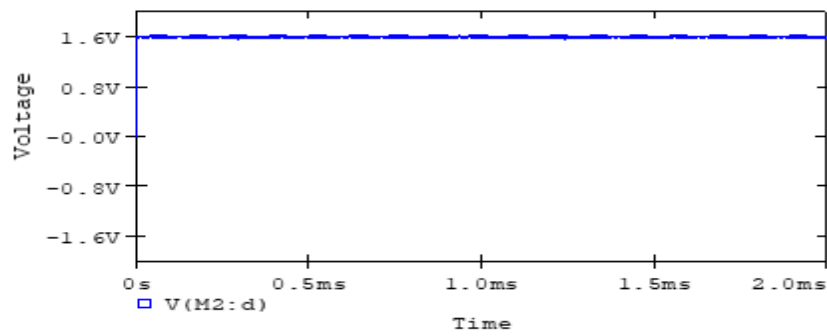
(a)
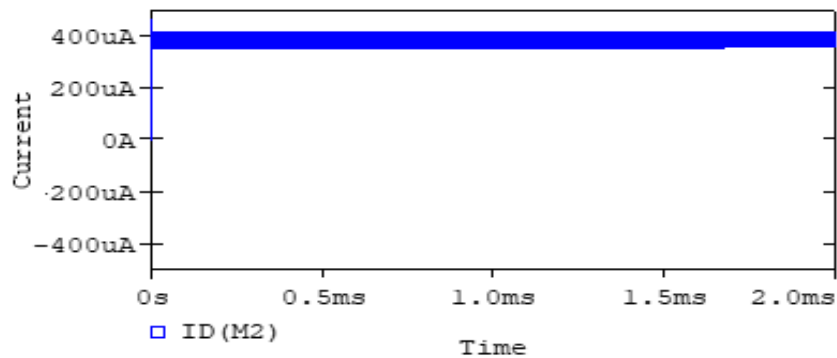
(b)

Fig. 4.7   Plot for MOSFET drain (a) voltage, and (b) current.

49
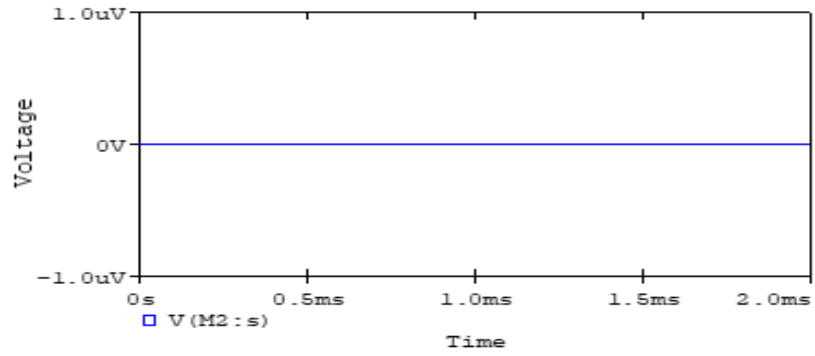
(a)
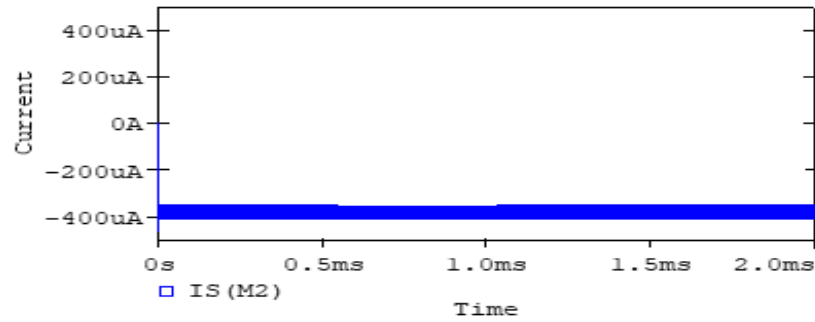
(b)

Fig. 4.8   Plot for MOSFET source (a) voltage, and (b) current.

Similarly, values of voltages and currents at sources and drain terminal have been deduced from plots at different values of reflection and recorded in Table 4.5. The MOSFET is said to have performed its function of absorbing reflected radio frequency signal if and only if the relationship $I_S \leq I_D$ and $V_{DS} = 0$ at the source terminal is satisfied, else, the model will fail.

Table 4.5.   Source and drain parameters deduced from plots

Reflected RF power P(dBm)	V_{DS} (*volts*) Source	V_{DS} (*volts*) Drain	I_s (*mA*)	I_D (*mA*)
3	0.00	0.002	0.0014	0.0014
5	0.00	0.0065	0.0027	0.0027
13	0.00	0.43	0.18	0.18
19	0.00	1.6	0.4	0.4

Using Table 4.5, in putting the values of voltages and current into the relationship $I_S \leq I_D$ and $V_{DS} = 0$, at different values of reflected power from port-4 of the circulator, the condition of MOSFET absorption was satisfied for all values of reflection from port-4 of the circulator as shown in Table 4.6.

Table 4.6.   Truth table condition for MOSFET absorption

Reflected power P(dBm)	V_{DS} at source terminal $= 0$	$I_S \leq I_D$
3	True	True
5	True	True
13	True	True
19	True	True

4.6   Conclusion

The proposed model has theoretically and practically confirmed that the destructive interference caused by reflection from the R_x branch of a 5G base station could be avoided using MOSFET technology to absorb reflected radio frequency signal. In addition to this, to verify the model's consistency, all values of reflection from port-4 of the circulator met with the condition for MOSFET absorption. Furthermore, a MOSFET was used in this model because it has the advantages of working as a passive element like resistor, capacitor, and inductor.

Chapter - 5

PERFORMANCE ANALYSIS OF PROPOSED MOSFET BASED ABSORBER FOR REFLECTED RF SIGNAL IN 5G M-MIMO BASE STATION

5.1   S-Parameter Analysis for Circulator and R_X Branch for the Proposed Model

Scattering parameters are mathematical construct used to characterize the performance of any electronic, electrical, or microwave network, especially at microwave and millimeter-wave region was equipment are not readily available to measure total voltage and current [113-116]. Furthermore, S-parameters are easier to measure at high frequencies, the measurement is direct and only involves measurement of relative quantities such as impedance, VSWR, return loss, voltage reflection coefficient incident, and reflected power at the connecting port in the system. Considering the four-port circulator (microwave device) used for the proposed model design, the S-parameter and resulting S-matrix have been generated for the four chosen reflection cases from the R_X branch circulator.

Parameters like VSWR, return loss, and R_X branch impedance have been calculated from the voltage reflection coefficient (S_{33}) deduced from the four-port circulator's S-matrix. In addition to this, the characteristic impedance is assumed to be *50 Ω*.
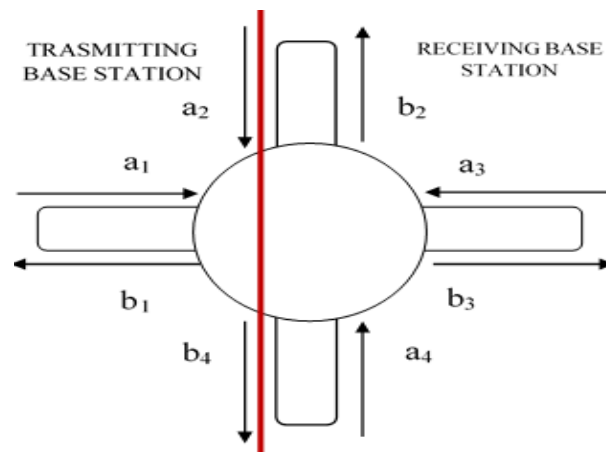
Fig. 5.1   incident and reflected voltage variable a and b.

$$a_n = \frac{incident \;\; voltage \; at \; n^{th} \; port}{\sqrt{characteristic \; impedance \; of \;\; n^{th} \; port}} \qquad (5.1)$$

$$b_n = \frac{reflected \; voltage \; at \; n^{th} \; port}{\sqrt{characteristic \; impedance \; of \;\; n^{th} \; port}} \qquad (5.2)$$

a_n and b_n are normalized incident and reflected voltage, respectively.

$$S_{Rj} = \frac{normalized \; reflected \; voltage \; at \; R^{th} \; port}{normalized \; incident \; voltage \; at \; j^{th} \; port}$$

$$S_{Rj} = \frac{b_{Rth} Port}{a_{Jth} Port} \qquad (5.3)$$

where R represents the normalized reflected voltage at the Rth port, while J represents the Jth port's normalized incident voltage. Considering *19 dBm* reflection loss the values of incident and reflected voltages at the different ports are recorded in Table 5.1.

Table 5.1. Incident voltage and reflected voltage at different ports

Port Number	Incident Voltage (*volts*)	Reflected Voltage (*volts*)
1	44.662	0
2	44.662	0
3	44.662	2.7
4	2.7	0

Using Table.5.1 the various S-parameters S_{33} have been calculated from values of a_3 and b_3 representing normalized incident and reflected voltage, respectively. These values a_3 and b_3 have been generated using Eq. (5.1) and Eq. (5.2):

$$a_n = \frac{incident \;\; voltage \; at \; n^{th} \; port}{\sqrt{characteristic \; impedance \; of \;\; n^{th} \; port}}$$

$$a_n = \frac{44.662}{\sqrt{50}} = \; 6.317$$

$$b_n = \frac{\textit{reflected voltage at } n^{th} \textit{ port}}{\sqrt{\textit{characteristic impedance of } n^{th} \textit{port}}}$$

$$b_n = \frac{2.7}{\sqrt{50}} = 0.38$$

The voltage reflection coefficient at *19 dBm* reflection loss has been deduced by substituting values of a_3 and b_3 into Eq. (5.3):

$$S_{Rj} = \frac{\textit{normalized reflected voltage at } R^{th} \textit{ port}}{\textit{normalized incident voltage at } j^{th} \textit{ port}}$$

$$S_{Rj} = \frac{0.38}{6.317}$$

$$S_{33} = 0.063$$

The voltage reflection coefficient, which is a function of the amount of power lost in the base station's T_X branch, has been used to calculate other parameters, as shown in the Section 5.2. To verify the value of voltage reflection coefficient deduced from the S matrix use:

$$\Gamma = 1 - \frac{P_d}{P_I} \tag{5.4}$$

where P_d, P_i, and P_r are power delivered, incident power, and reflected power, respectively. The values of P_i and P_r are *20 Watts and 0.079 Watts,* respectively. Substitute values of P_i and P_r into (6): $\Gamma = 0.063$.

This value is equal to the value obtained from the S-matrix. The parameter can also be called a transmission coefficient as it describes the amplitude, intensity, or total power of a transmitted wave relative to an incident wave as captured in Fig 5.1.

5.2 Methods of Quantifying Level of Reflected Power Calculated

As stated in the proposed model, the major cause of reflection in the base station's R_X branch is the difference in load and source impedances. The source impedance has been defined to be *50 Ω.* To calculate the load impedance, the used formula is [26, 106, 117]:

$$\Gamma = \frac{Z_L - Z_O}{Z_L + Z_O} \tag{5.5}$$

Where Γ is the voltage reflection coefficient, Z_L is Load impedance and Z_L is Source impedance, Recall: $S_{33}= \Gamma =0.063$ and $Z_O= 50 \ \Omega$. Substituting the values of Z_O and Γ into Eq. (5.5) , Z_L is calculated as *56.7235* Ω.

Two methods have been used to quantify the level of reflected power from the base station's R_X branch, the return loss, and the VSWR. The impedance mismatch between the T_X and R_X branch creates a high VSWR, causing the signal to be reflected [118], [119]. The VSWR for 19 dBm reflection loss can be computed using Eq. (5.6):

$$\Gamma = \frac{Vswr-1}{Vswr+1} \tag{5.6}$$

Substituting the value of voltage reflection coefficient into Eq. (5.6):

$$0.063(Vswr+1) = Vswr-1$$

$$Vswr = 1.34:1$$

The return loss is the difference in dB between the transmitted power and the reflected power. The larger the value of the return loss, the less power reflected. The required return loss to be as large as possible, and it must always be a positive number. Now, return loss is given by [120] :

$$Re\,turn\ loss \ = \ -20\log\left(\frac{Vswr-1}{Vswr+1}\right) \tag{5.7}$$

Substitute value of VSWR into Eq. (5.7)

$$Re\,turn\ loss \ = \ -20\log\left(\frac{1.34-1}{1.34+1}\right)$$

$$Re\,turn\ loss \ = \ 24.042 \ dB$$

Values of return loss, VSWR Impedances, and voltage reflection coefficient have been calculated for other cases of reflection from the R_X branch and recorded in Table 5.2.

Table. 5.2   Summary of parameters at different cases of reflection from the R_X branch

Incident power (*dBm*)	Reflected Power (*dBm*)	Reflected Power (*Watt*)	VSWR	Impedance (Ω)	Return Loss (*dB*)	Reflection Coefficient
43	3	0.002	1.001:1	50.01001	60	0.0001
43	5	0.0032	1.0263:1	51.31712	37.735	0.013
43	13	0.02	1.0652:1	53.263	30	0.0316
43	19	0.079	1.134:1	56.7325	24.024	0.063

Conclusively, the values of parameters calculated for the various chosen reflections depend on the value of the voltage reflection coefficient deduced from the circulator's S-matrix. From Table 5.2, the VSWR for each case is within the acceptable value, and in cases where reflection increases, the VSWR increases. In addition to this, VSWR's value may change if the connection between the circulator and the R_X branch is not tight or corrosion in the circulator's joint. When this happens, not all the reflected power will get to the drain terminal of the MOSFET. It will reduce the MOSFET's efficiency since the efficiency of the MOSFET is a function of total power absorbed.

5.3   Performances Analysis of Proposed Model

The proposed model circuit's performance has been analysed as a two-port network with port-4 of the circulator used as port-1 while the source terminal of the MOSFET is tagged the port-2 of the network. Efficiency, insertion loss, total power absorbed by MOSFET, total power loss to the rectifier, and reflection coefficient, which can be used to determine the return loss, have been analysed.

5.3.1 Parameter analysis

As stated in Chapter 4, Scattering parameters are mathematical constructs used to characterize the performance of any electronic, electrical, or microwave network, especially at microwave and millimeter-wave frequencies where equipment is not readily available to measure total voltage and current [121]. The S-parameters have been calculated for the four chosen cases of reflection from port-3 of the circulator to do a proper analysis.

$$S_{11} = \frac{\mathrm{Re}\ flected\ power\ at\ port\text{-}1}{incident\ power\ at\ port\text{-}1} \qquad S_{12} = \frac{Transmitted\ power\ to\ port\text{-}1}{incident\ power\ at\ port\text{-}2}$$

$$S_{21} = \frac{Transmitted\ power\ to\ port\text{-}2}{incident\ power\ at\ port\text{-}1} \qquad S_{22} = \frac{\mathrm{Re}\ flected\ power\ at\ port\text{-}2}{incident\ power\ at\ port\text{-}2}$$

Now, reflected power at port-1 is calculated as:

$$\mathrm{Re}\ flected\ power\ at\ port\text{-}1\ =\ RITC \times RITV \tag{5.8}$$

where RITC and RITV represent rectifier input terminal current and rectifier input terminal voltage, respectively. From Table 4.5, rectifier input terminal current and voltage are *1.33 mA* and *2.7 Volts,* respectively. Substituting values of RITC and RITV into Eq. (5.8), reflected power at port-1 is *0.00359 W.* But reflected power at port-2 is calculated as:

$$\text{Re}\,flected\ power\ at\ port\text{-}2\ =\ STC \times VDMC \qquad (5.9)$$

where STC and VDMC represent source terminal current and voltage drop along the MOSFET channel, respectively. Table 4.5 shows that source terminal current and voltage drop across the MOSFET channel is *0.4 mA* and *1.6 Volts* respectively. Substituting these values into Eq. (5.9), reflected power at port-2 is *0.064 mW:*

$$Transmitted\ power\ to\ port\text{-}1\ =\ incident\ on\ port\text{-}1\ -\ reflected\ at\ port\text{-}1 \qquad (5.10)$$

$$Transmitted\ power\ to\ port\text{-}1\ = 20 - 0.003591$$

$$Transmitted\ power\ to\ port\ 1 = 0.00359\ W$$

To calculate power transmitted to port-2 use:

$$Transmitted\ power\ to\ port\text{-}2\ = \text{Re}\,flected\ at\ port\text{-}1\ \text{-}\ \text{Re}\,flected\ at\ port\text{-}2 \qquad (5.11)$$

$$Transmitted\ power\ to\ port\text{-}2\ = 0.00359 - 0.00064$$

$$Transmitted\ power\ to\ port\ 2 = 0.00295\ W$$

But *Incident power on port 1 = 20 Watt and   Incident power on port 2 = 0 Watt.* Now:

$$S_{11} = \frac{0.00359}{20} = 0.000179$$

S_{11} is the reflection coefficient

$$S_{12} = \frac{19.996}{0} = 0 \qquad S_{21} = \frac{0.00295}{20} = 0.0001475 \qquad S_{22} = \frac{0.0658}{0} = 0$$

$$s = \begin{pmatrix} s_{11} & s_{12} \\ s_{21} & s_{22} \end{pmatrix} = \begin{pmatrix} 0.000179 & 0 \\ 0.000148 & 0 \end{pmatrix} \qquad \begin{matrix} b_1 \\ b_2 \end{matrix} = \begin{pmatrix} s_{11} & s_{12} \\ s_{21} & s_{22} \end{pmatrix} \cdot \begin{pmatrix} a_1 \\ a_2 \end{pmatrix}$$

The s matrix of the proposed model under *19 dBm* reflection from port-3 going out through port-4 of the circulator is given as:

$$s = \frac{b_1}{b_2} = \begin{pmatrix} 0.000179 & 0 \\ 0.000148 & 0 \end{pmatrix} \cdot \begin{pmatrix} 20 \\ 0 \end{pmatrix}$$

Total power reflected at port1 (Outbound power) =TPRP1

$$TPRP1 = b_1 = S_{11}a_1 + S_{12}a_2 \tag{5.12}$$

$$TPRP1 = b_1 = 0.000179 \times 20 + 0 \times 0 = 0.003591$$

$$TPRP1 = b_1 = 0.003591 \; Watts$$

Total power reflected at port2 (Out bound power) =TPRP2

$$TPRP2 = b_2 = S_{21}a_1 + S_{22}a_2 \tag{5.13}$$

$$TPRP2 = b_2 = 0.000148 \times 20 + 0 \times 0 = 0.00295 \; Watts$$

5.3.2 Insertion loss

The insertion loss measures the amount of energy lost when a signal arrives at a receiver. It is also defined as the attenuation or loss of signal power resulting from a component [122]. A MOSFET based absorber has been inserted between the T_X and R_X branch of the base station constructs. This parameter is only defined as a two-port network. The insertion loss is given by [122]:

$$Insertion.loss = 10\log(s_{21}) = 10\log\left(\frac{P_{out}}{P_{in}}\right) \tag{5.14}$$

S_{21} has been calculated as 0.000148.

$$Insertion.loss = 10\log(0.000148)$$

$$Insertion \; loss = 38.3 dB$$

Previously, engineers used the term attenuation to characterize absorption of an absorber, but insertion loss is now the accepted standard for characterizing absorption levels. We want the insertion loss of any absorber model to be as high as possible.

Performance parameter analysis has been carried out for other chosen cases of reflection from port-3 going out through port-4 of the circulator, and the results are captured in Table. 5.2.

5.3.3 Efficiency

The proposed model's efficiency has been calculated as a function of the total power absorbed by the MOSFET, total power loss to the rectifier circuit, and the reflected power from port-4 of the circulator as:

$$Efficiency = \frac{TPAM + TPLR}{\text{Re} \, flected \, power \, from \, port \, 4 \, of \, circulator} \times \frac{100}{1} \tag{5.15}$$

The TPAM and TPLR are total power absorbed by MOSFET and total power loss to the rectifier circuit.

$$TPAM = source \, ter \min al \, current \, \times \, voltage \, drop \, along \, the \, MOSFET \, channel$$

$$TPAM = STC \times VDMC \tag{5.16}$$

$$TPAM = 0.4 \times 0.001 \times 1.6$$

$$TPAM = 0.00064 \, Watt$$

This is equal to the reflected power at port-2, as presented in chapter 5.3.1.

$$TPLR = \text{Re} \, al \, rectifier \, input \, ter \min al \, power \, - \, TPAM \tag{5.17}$$

where rectifier input terminal power is a function of Real rectifier input terminal current, and voltage as presented as:

$$\text{Re} \, al \, rectifier \, input \, ter \min al \, power = RITC \times RITV \tag{5.18}$$

From Table. 4.5, rectifier input terminal current and voltage are *1.33 mA* and *2.7 Volts*, respectively. Substituting these values into Eq. (18)

$$\text{Re} \, al \, rectifier \, input \, ter \min al \, power = 1.33 \times 0.001 \times 2.7$$

$$\text{Real rectifier input terminal power} = \textit{0.00359 Watt}$$

This value is equal to the value of power reflected at port-1. Now, substituting values of TPAM and real rectifier input terminal power into Eq. (5.17), we have:

$$TPLR = 0.00359 - 0.00064$$

$$TPLR = 0.00295 \, Watt$$

Now, to calculate the efficiency of the proposed model, substitute values of TPRL, TPAM, and reflected power from the circulator into Eq. (5.15); Efficiency becomes*:*

$$Efficiency = \frac{0.00064 + 0.00295}{0.00359} \times \frac{100}{1}$$

$$Efficiency = 100 \%$$

Table. 5.3   Summary of proposed model performance

Reflected Power(*dBm*)	Reflected Power(*mW*)	Insertion loss (*dB*)	Efficiency (%)	TPAM (*mW*)	TPLR (*mW*)	Reflection Coefficient
3	0.004	57.1	> 90	0.00008	0.00392	0.0000002
5	0.0152	61.2	>90	0.000017	0.01518	0.00000076
13	0.2448	32.2	>90	0.0774	0.1674	0.00001224
19	3.59	38.3	>90	0.64	2.95	0.000179

However, the rectification process forms part of the absorption process of RF power, for this reason, it can be assumed that the rectifier and MOSFET absorb all the power reflected from the port- 3 of the circulator, and collectively, it can be said that the model, in general, is near *100 %* efficient as *100 %* efficiency is not achievable in practice.

5.4   Comparative Analysis of the Proposed Model with Existing Models

To validate the proposed model's efficacy, comparisons have been made with absorber models, which exist as RF absorbers, microwave absorbers, EMI absorbers, and radar absorbing materials or surface wave absorbers [123, 124]. All these different nomenclatures point to a material whose magnetic or electric properties have been altered to attenuate or absorb energy. This comparison has been captured in Table 5.4.

The proposed model's main target is efficiency at any chosen frequency, especially in the 5G era, where the highest efficiency at the selected frequency band is a target for telecom companies. Table 5.4 shows that the proposed model has its strength in its efficiency, which depends on the power absorbed by the MOSFET and the power lost to the rectifier circuit. In addition to this, it also has the advantage of absorbing RF power at any frequency depending on the frequency at which the rectifier was designed to handle.

Table 5.4 Comparison of proposed model with Existing models

Reference	Efficiency (%)	Frequency (GHZ)	Insertion loss (dB)
[75]	> 90	12 – 18	< 10
[76]	--	4 - 13.5	> 10
[77]	--	4.23 – 8.13	< 10
[78]	> 90	9.5 – 55	--
[79]	75	2 – 7	< 10
[80]	94.7	5.9	< 15
[81]	--	2.5 – 5.5	< 10
[82]	--	7.56 - 14.58	< 10
[83]	--	8 – 12	< 10
[84]	90	2 – 5	--
This work	> 90	28	> 38

5.5   Conclusion

One key concern of 5G technology is maximum efficiency at any level of constrain. Using a MOSFET-based absorber to solve the 5G base station reflection effects has proved to be highly efficient compared to other existing models of absorbers in terms of RF power level they can absorb, efficiency, and allowable frequency ranges as recorded in Table 5.4. The proposed model has also provided almost a *100 %* efficiency and an insertion loss greater than *38 dB* at all chosen instances of reflection from the circulator and a varying frequency range. Apart from all these key advantages, another key feature of the proposed model is its ease of implementation.

Chapter - 6
CONCLUSIONS AND FUTURE WORKS

6.1 Conclusions

Interference caused by signal reflections from a circulator in the 5G base station (for unmatched termination between the T_X branch and R_X branch) has been analysed. The proposed model has theoretically proved that destructive interference caused by reflection from the R_X branch can be avoided by using MOSFET technology to absorb the signal. Various current and voltage relationships of the reflected signal have been established for the proposed model in this work. In addition to this, to verify the model's consistency, all values of reflection from port 4 of the circulator met with the condition for MOSFET absorption, as presented in Table 4.6.

Considering Table 4.2 and Table 4.3, a voltage drop from *2.7 Volts* to *1.8 Volts* as a result of the resistive components present in the rectifier of the proposed model construct. Ideally, the value of voltage and current at the rectifier output is supposed to be the same value as the drain terminal current and voltage value of the MOSFET but taking a close look at Tables 4.3 and 4.5, the value of voltage and current drop from *1.8 Volts* and *0.9 mA* to *1.6 Volts* and *0.4 mA* respectively. This variation in the output terminal of the rectifier output and drain terminal parameters results from the operating condition of MOSFET at a high frequency. Although the chosen values of reflected power in *dBm* are large, these values have been chosen for experimental purposes to get a voltage component that can be applied to the rectifier's input terminal as presented in Table 4.1.

However, considering Tables 4.2 and Table 5.3, the real reflected power is small compared to the theoretical value of power for each of the chosen cases of reflection from the R_X branch of circulators in the base station, and all parameter analysis has been carried out with the real values of the power, voltage, and current. Also, this value of reflected power is different from the watt value of *19 dBm* reflected power, this value was obtained from the input plot after applying a voltage of *2.7 Volts*, which is the voltage component of the assumed reflected power. Using these values of reflected power and its voltage and current components, parameters such as VSWR, impedance, return loss, and voltage reflection coefficient have been calculated using the theoretical value of power reflected for the different reflection cases from the R_X branch as captured in Table 5.2. From

Table.5.2, it has been observed that as the reflection level increases, the VSWR and impedance increase, but this increase is within acceptable limits for the chosen cases of reflection. Also, VSWR's value may change if the connection between the circulator and the R_X branch is not tight or corrosion in the circulator's joint.

Considering Table 5.3, the insertion loss measurement, which is one of the critical measurements used to analyse the proposed model's performance quality, has been observed to be high at different levels of reflection from the base station's Rx branch. The real reflected power has been used to predict this parameter performance of the proposed model. This parameter has been observed to be high when the amount of power reflected from the R_X branch is low, as presented in Table 5.3. Also captured in Table 5.3 is the efficiency of the proposed model, which has been calculated using the real value of reflected power from the R_X branch, it is observed that the efficiency of the proposed model is almost *100 %* because the rectifier and MOSFET are fundamental parts of the proposed model construct.

Conclusively, the key concern of 5G technology is maximum efficiency at any level of constrain. Using a MOSFET-based absorber to solve the 5G base station reflection effects has proved to be highly efficient compared to other existing models of absorbers in terms of RF power level they can absorb, efficiency, and allowable frequency presented in Table 5.4. The proposed model has provided almost a *100 %* efficiency and an insertion loss greater than *38.3 dB* at all chosen instances of reflection from the circulator and an operating frequency of *28 GHz*.

Key performance parameters have been presented in Table. 6. From table, it has been observed that as the load impedance or R_X branch impedance increases, the level of reflected power increases with a decrease in the return loss.

<p align="center">Table. 6.1   Summary of key performance parameters</p>

Reflected Power(*dBm*)	Load Impedance (Ω)	Insertion loss (*dB*)	Efficiency (%)	TPAM (*mW*)	TPLR (*mW*)	Return losss (*dB*)
3	50.01	57.1	> 90	0.000080	0.003920	60.000
5	51.32	61.2	>90	0.000017	0.015180	37.735
13	53.26	32.2	>90	0.077400	0.167400	30.000
19	53.73	38.3	>90	0.640000	2.950000	24.024

6.1.1 Advantages of proposed model

- One key advantage, and feature of the proposed model is its ease of implementation.
- The model can be designed to operate at any frequency depending on the frequency at which the rectifier in the model is designed.
- The model can provide a very high insertion loss because the model absorbs all the power reflected from the R_X branch.
- The proposed model is cost-effective.
- The proposed model has been proven to be a solution to telecom engineers' problems when designing an impedance matching circuit between the T_X and R_X branch of a base station.

6.1.2 Disadvantages of proposed model

- As a result of the presence of components such as resistors, capacitors inductors, and MOSFET, there may be a need for a cooling system to increase the model's life span.

6.1.3 Challenges encountered during simulation

- During the simulation process, because of the high frequency, too much time has been spent on simulation to get the required result.
- There was an insufficient model for circulator port simulation, for this reason, a sinusoidal voltage source and voltage divider was used to provide an equivalent value of reflected power from the R_X branch of the circulator.

6.2 Future Works

The future work of this research is to physically implement the proposed model by using a MOSFET that can operate effectively at *28 GHz*. On the physical implementation, a circulator will be used to provide a real port to the port connection between the R_X branch and the branch connected to the absorber. Since, at high frequency, it becomes difficult to analyse the concept of voltages and currents, especially when discrete electronic components are present in the circuit. To mitigate these effects, a combination of high-

frequency electronic devices, Schottky diode, and high-frequency MOSFET will be used for the physical implementation of the proposed model construct.

Furthermore, this model's physical implementation will allow for comparison between the simulated values of the performance parameters and real values in cases where there is a direct port to port connection. This comparison will enable Engineers to determine the proposed model's reliability and sustainability compared to previously existing RF absorber models.

REFERENCES

[1]   H. Jaakkola, "Mobile telephones-the way towards the penetrated markets, "*IEEE International Engineering Management Conference*, Cambridge, UK, vol.1, pp. 67-72 vol, Aug. 2002.

[2]   G. Heine, H. Sagkob, "GPRS: Gateway to Third Generation Mobile Networks," *Artech House*, Feb. 2003.

[3]   J. Huang, S. Su, and J. Chen, "Design and performance analysis for data transmission in GSM/GPRS system with voice activity detection " *IEEE Transactions on Vehicular Technology*, vol. 51, no. 4, pp. 648-656, July 2002.

[4]   Y. Rao, W. Yeung, and A. Kripalani, "Third-generation (3G) radio access standards," *International Conference on Communication Technology Proceedings*, Beijing, China, vol.2, pp. 1017-1023, August 2002.

[5]   A. Khlass, S. Elayoubi, and T. Bonald, "Capacity gains from multipoint single frequency transmission in HSPA+," *IEEE Wireless Communications and Networking Conference (WCNC)*, Shanghai, pp. 476-480, April 2013,

[6]   S. Yi, S. Chun, Y. Lee, S. Park, S. Jung, "Overview of LTE and LTE-Advanced new features," *Radio Protocols for LTE and LTE-Advanced*, *Wiley*, pp.151-158, August 2012.

[7]   N. Mitra, P. Agrawal, "5G mobile technology: A survey," *ICT Express*, vol. 1, no. 3, pp. 132-137, Dec. 2015

[8]   S. Parkvall, E. Dahlman, A. Furuskar, and M. Frenne, "NR: The New 5G radio access technology," *IEEE Communications Standards Magazine*, vol. 1, no. 4, pp. 24-30, Dec. 2017.

[9]   J. Isabona and Viranjay M. Srivastava, "Downlink massive MIMO systems achievable sum rates and energy efficiency perspective for future 5G systems," *Wireless Personal Communication (WPC)*, vol. 96, no. 2, pp. 2779-2796, Sept. 2017.

[10]   Rath Vannithamby and Shilpa Talwar, "Towards 5G: Applications*, Requirements and Candidate Technologies*, Wiley, Jan. 2017.

[11]   S. Praptodiyono, I. Hasbullah, R. Murugesan, and S. Ramadass, "Survey of internet protocol version 6 link local communication security vulnerability and mitigation methods*," IETE Technical Review*, vol. 30, no. 1, pp. 64-71, Jan.-Feb. 2013.

[12]   C. Hoymann, D. Astely, M. Stattin, G. Wikstrom, J. Cheng, A. Hoglund, M. Frenne, R. Blasco, J. Huschke, and F. Gunnarsson, "LTE Release 14 Outlook," *IEEE Communications Magazine*, vol. 54, no. 6, pp. 44-49, June 2016.

[13]   Joseph Isabona, Viranjay M. Srivastava, and Omashere O. Robert, "Spatial variation of the electromagnetic radiations due to exposure to telecommunication base station transmitters in a pilot region," *Int. J. of Applied Engineering Research,* vol. 11, no. 22, pp. 10994-11001, Dec. 2016.

[14]   David Muirhead, M. Imran, and Kamran Arshad, "A survey of the challenges, opportunities and use of multiple antennas in current and future 5G small cell base stations," *IEEE Access*, vol. 4, pp. 2952-2964, May 2016.

[15]   B. Yoo, J. Park, and J. Yang, "Quasi-circulator using an asymmetric coupler for Tx leakage cancellation," *Multidisciplinary digital publishing institute(MDPI*), Basel, Switzerland, Sept. 2018

[16]   C. Chang, Yu. Lo, and J.Kiang, "A 30 GHz active quasi-circulator with current-reuse technique in 0.18 μm CMOS technology," *IEEE Microwave and Wireless Components Letters*, vol. 20, no. 12, pp. 693-695, Dec. 2010.

[17]   Sen Wang, C. Lee, and Y. Wu, "Fully integrated 10-GHz active circulator and quasi-circulator using bridged-T networks in standard CMOS," *IEEE Transactions on Very Large Scale Integration (VLSI) Systems*, vol. 24, no. 10, pp. 3184-3192, Oct. 2016.

[18]   Shih C. Shin, Jhih Y. Huang, Kun Y. Lin, and Huei Wa, "A 1.5–9.6 GHz monolithic active quasi-circulator in 0.18 μm CMOS technology," *IEEE Microwave And Wireless Components Letters*, vol. 18, no. 12, pp. 797-799, Dec. 2008.

[19]   S. Seyyed, Amir Ayati, Debashis Mandal, Bertan Bakkaloglu, and Sayfe Kiaei, "Adaptive integrated CMOS circulator," *IEEE Radio Frequency Integrated Circuits Symposium (RFIC)*, San Francisco, CA, USA, pp. 146-149, May 2016,

[20]   Tolga Dinc and Harish Krishnaswamy, "A 28GHz Magnetic-free non-reciprocal passive CMOS circulator based on spatio-temporal conductance modulation,"

IEEE International Solid-State Circuits Conference, San Francisco, CA, USA, pp. 294-296, 5-9 Feb. 2017.

[21] S. Jeon, K. Yoo, Y. Kim, and J. Cheon, "Advanced impedance matching technology to optimize RF circuit design of practical wireless systems," *Asia-Pacific International Symposium on Electromagnetic Compatibility (APEMC)*, Seoul, pp. 328-330, July 2017.

[22] N. Morikoshi, Ryo Yokota, Takafumi Kuramoto, Shinichi Uchida, Tomoyuki Tanaka, Yoshiyuki Ota, Mitsuru Hiraki, Mitsuru Hiraki, and Takahiro Nakamura, "Design of on-board impedance matching circuit for millimeter-wave presystem," *12th Global Symposium on Millimeter Waves (GSMM)*, Sendai, Japan, pp. 59-61, May 2019,

[23] M. Added and N. Boulejfen, "Variable impedance matching network based on varactor diodes," *2015 IEEE 15th Mediterranean Microwave Symposium (MMS)*, Lecce, pp. 1-4, Nov. 2015,

[24] A. S. Sedra and K. C. Smith, *Microelectronic Circuits: Theory and Applications*, 7th Ed. Oxford University Press, 2014.

[25] R. L. Boylestad and L. Nashelsky, *Electronic devices and circuit theory*, 11th Ed. Pearson Prentice Hall, 2012.

[26] Viranjay M. Srivastava and G. Singh, *MOSFET technologies for double-pole four throw radio frequency switch*, Springer International Publishing, Switzerland, Oct. 2013.

[27] Petri Launiainen, *A Brief History of Everything Wireless*, 1st Ed. Springer International Publishing, 2018.

[28] Murat Uysal, Carlo Capsoni, Zabih Ghassemlooy, Anthony Boucouvalas, and Eszter Udvary, *Optical Wireless Communication*, 1st Ed. Springer International Publishing, Switzerland 2016.

[29] H. Frank, P. Fitzek, Marcos D. Katz, "Wireless communication technologies," *Mobile Clouds: Exploiting Distributed Resources in Wireless, Mobile and Social Networks*, Wiley, pp.53-66. Dec. 2014

[30] Nathan Blaunstein, Christos G. Christodoulou, "Antenna fundamentals," *Radio Propagation and Adaptive Antennas for Wireless Communication Networks*, Wiley, pp.34-53, April 2014.

[31] Z. Zhou, Z. Wei, Z. Tang, and Y. Yin, "Design and analysis of a wideband multiple-microstrip dipole antenna with high isolation," *IEEE Antennas and Wireless Propagation Letters*, vol. 18, no. 4, pp. 722-726, April 2019.

[32] Norihiko Morinag, Ryuji Kohno, and Seiichi Sampei, *Wireless communication technologies: New multiMedia systems*, Springer International Publishing, 2002.

[33] D. Fang, Y. Qian, and R. Q. Hu, "Security for 5G mobile wireless networks," *IEEE Access*, vol. 6, pp. 4850-4874, Dec. 2018.

[34] W. Bailey, B. Cotts, and P. Dopart, "Wireless 5G radio frequency technology, an overview of small cell exposures, standards and science," *IEEE Access*, vol. 8, pp. 140792-140797, July 2020.

[35] Abdulrahman Yarali, *Public Safety Networks from LTE to 5G*, Wiley, pp.189-194, Dec 2020.

[36] Anwer Al-Dulaimi, Xianbin Wang, Chih Lin, "5G networks fundamental requirements, enabling technologies, and operations management", *IEEE*, pp.299-326, Oct. 2018.

[37] Andreas F. Molisch, "Technical Challenges of Wireless Communications*" IEEE*, pp.27-36, 2011.

[38] S. Dutta Roy, "Characteristics of single- and multiple-frequency impedance matching networks, "*IEEE Transactions on Circuits and Systems*, vol. 62, no. 3, pp. 222-225, March 2015.

[39] A. Jurkov, A. Radomski, and D. Perreault, "Tunable matching networks based on phase-switched impedance modulation1," *IEEE Transactions on Power Electronics*, vol. 35, no. 10, pp. 10150-10167, Oct. 2020.

[40] Y. Zheng and C. Saavedra, "Active quasi-circulator MMIC Using OTAs," *IEEE Microwave and Wireless Components Letters*, vol. 19, no. 4, pp. 218-220, April 2009.

[41] Edward A. Ohm, "A broad-band microwave circulator," *IRE Transactions on Microwave Theory and Techniques*, vol. 4, no. 4, pp. 210-217, Oct. 1956.

[42] Douglas K. Linkhart, *Microwave Circulator Design*, 2nd Ed., Artech House, Bostan, 2014.

[43] N. Sugimoto, T. Shintaku, A. Tate, H. Terui, M. Shimokozono, E. Kubota, M. Ishii, and Y. Inoue, "Waveguide polarization-independent optical circulator," *IEEE Photonics Technology Letters*, vol. 11, no. 3, pp. 355-357, March 1999.

[44] T. Hao, Z. Dong, and Q. Huang, "design of *1.9GHz-2.6GHz* microstrip circulator based on ferrite material" *International Symposium on Antennas, Propagation and EM Theory (ISAPE)*, Hangzhou, China, pp. 1-3, Dec. 2018,

[45] M. Pinto, L. Marzall, A. Ashley, D. Psychogiou, and Z. Popovic, "Design-oriented modelling of microstrip ferrite circulators," *European Microwave Conference (EuMC)*, Madrid, pp. 215-218, Sept. 2018,

[46] Harish Krishnaswamy, "A breakthrough millimeter-wave, non-magnetic circulator," *Nature Communication*, October 2017,

[47] M. Nafe, X. Wu and X. Liu, "A wideband magnetic-free circulator using spatio-temporal modulation of 2-pole bandpass filters," *IEEE Radio and Wireless Symposium (RWS)*, Orlando, FL, USA, pp. 1-3, Jan. 2019.

[48] T. Dinc, A. Nagulu and H. Krishnaswamy, "A millimeter-wave non-magnetic passive SOI CMOS circulator based on spatio-temporal conductivity modulation," *IEEE Journal of Solid-State Circuits*, vol. 52, no. 12, pp. 3276-3292, Dec. 2017.

[49] C. Yang and P. Gui, "On-chip 100GHz full-duplex circulator/duplexer design based on non-reciprocal transmission line," Symposium on Wireless and Microwave Circuits and Systems (WMCS), Waco, TX, pp. 1-4, April 2018.

[50] O. Leisten, R. Collier, and R. Bates, "Distributed amplifiers as duplexer/circulator components at S-band," *IEE Colloquium on Solid-State Components for Radar*, London, UK, pp. 5/1-5/4, Feb. 1988.

[51] F. Barradas, T. Cunha, P. Cabral, and J. Pedro, "Magnetless RF isolator design using grounded transistors," *IEEE/MTT-S International Microwave Symposium - IMS*, Philadelphia, PA, pp. 439-442, Aug. 2018.

[52] F. Ghaffar, M. Vaseem, J. Bray and A. Shamim, "A half mode inkjet printed tuneable ferrite isolator," *IEEE MTT-S International Microwave Symposium (IMS),* Honolulu, HI, pp. 289-291, Oct. 2017.

[53] W. Marynowski, "Integrated broadband edge-guided mode isolator with antiparallel biasing of the ferrite Slabs," *IEEE Microwave and Wireless Components Letters*, vol. 28, no. 5, pp. 392-394, May 2018.

[54] N. Landsberg and E. Socher, "An F-band reflection amplifier using 28 nm CMOS FD-SOI technology for active reflectarrays and spatial power combining applications," *IEEE MTT-S International Microwave Symposium (IMS)*, San Francisco, CA, pp. 1-3, May. 2016.

[55]   M. Steer, "Gain saturation in circulator-coupled reflection amplifiers," *IEEE MTT-S International Microwave Symposium Digest*, USA, pp. 395-398, 1985.

[56]   M. Porranzl, C. Wagner, H. Jaeger, and A. Stelzer, "An active quasi-circulator for 77 GHz automotive FMCW radar systems in SiGe technology," *IEEE Microwave and Wireless Components Letters*, vol. 25, no. 5, pp. 313-315, May 2015.

[57]   N. Nakamoto, T. Takahashi, T. Nomura, M. Otsuka, and H. Miyashita, "A method to measure the antenna mode and structural mode for antenna RCS reduction using circulator and phase shifter," *International Symposium on Antennas and Propagation Conference Proceedings*, Kaohsiung, pp. 21-22, Dec. 2014,

[58]   O. Hiari and R. Mesleh, "Impact of RF–switch insertion loss on the performance of space modulation techniques," *IEEE Communications Letters*, vol. 22, no. 5, pp. 958-961, May 2018.

[59]   C. Chappidi, T. Sharma and K. Sengupta, "Multi-port active load pulling for mm-Wave 5G power amplifiers: bandwidth, back-off efficiency, and VSWR tolerance," *IEEE Transactions on Microwave Theory and Techniques*, vol. 68, no. 7, pp. 2998-3016, July 2020.

[60]   N. Sugimoto, T. Shintaku, A. Tate, H. Terui, M. Shimokozono, E. Kubota, M. Ishii, and Y. Inoue, "Waveguide polarization-independent optical circulator," *IEEE Photonics Technology Letters,* vol. 11, no. 3, pp. 355-357, March 1999.

[61]   C. E. Fay and R. L. Comstock, "Operation of the ferrite junction circulator," IEEE Transactions on microwave theory and techniques, vol. 13, no. 1, pp. 15-26, Jan. 1965.

[62]   M. Darques, J. De la Torre Medina, L. Piraux, L. Cagnon, and I. Huynen, "Microwave circulator based on ferromagnetic nanowires in an alumina template," Nanotechnology, vol. 21, no. 14, April 2010.

[63]   Q. Zhang, Z. Shen, J. Wang, and K. S. Lee, "Design of a switchable microwave absorber," *IEEE Antennas and Wireless Propagation Letters*, vol. 11, pp. 1158-1161, 2012.

[64]   André Vorst, Arye Rosen, and Youji Kotsuka, *RF/Microwave interaction with biological tissues*, Willey, Dec. 2005.

[65]   Y. Li, D. Li, H. Luo, F. Chen, X. Wang, and R. Gong, "Co-evaluation of reflection loss and surface wave attenuation for magnetic absorbing material*," IEEE*

Transactions on Antennas and Propagation, vol. 66, no. 11, pp. 6057-6060, Nov. 2018.

[66]   Y. Okano, S. Ogino and K. Ishikawa, "Development of optically transparent ultrathin microwave absorber for ultrahigh-frequency RF identification system," *IEEE Transactions on Microwave Theory and Techniques*, vol. 60, no. 8, pp. 2456-2464, Aug. 2012.

[67]   M. Asghar, S. Gowdu, J. Nagel, F. Baumgärtner, R. Stephan and M. Hein, "Evaluation of absorber configuration for a low clutter environment for over-the-air automotive radar testing," *IEEE MTT-S International Conference on Microwaves for Intelligent Mobility (ICMIM),* Detroit, MI, USA, pp. 1-4, June 2019

[68]   S. Ghosh and K. Srivastava, "Polarization-insensitive dual-band switchable absorber with independent switching," *IEEE Antennas Wireless Propagation. Letters.*, vol. 16, pp. 1687-1690, Feb. 2017.

[69]   B. Hagen, *Radio frequency electronics circuit and application*, 2nd Ed. Cambridge University Press, June 2009.

[70]   Daniel B. Talbot, *Practical analog and RF electronics*: CRC press, 2000.

[71]   D. Houtz and D. Gu, "A Measurement technique for infrared emissivity of epoxy-based microwave absorbing materials," *IEEE Geoscience and remote sensing letters*, vol. 15, no. 1, pp. 48-52, Jan. 2018.

[72]   Qian X and Yi Huang, "Theory for anechoic chamber design," *IEEE*, pp.11-33, 2018.

[73]   G. Luo, W. Yu, Y. Yu, X. Zhang, and Z. Shen, "A Three-dimensional design of ultra-wideband microwave absorbers," *IEEE Transactions on Microwave Theory and Techniques*, vol. 68, no. 10, pp. 4206-4215, Oct. 2020.

[74]   Q. Zhang, Z. Shen, J. Wang, and K. S. Lee, "Design of a switchable microwave absorber," *IEEE Antennas and Wireless Propagation Letters*, vol. 11, pp. 1158-1161, Sep. 2012.

[75]   D. Hu, H. Zhai, S. Li, W. Xiong, and L. Zhang, "A new miniaturized absorber frequency selective surface for low frequency wave transmission and high frequency absorption," *International Conference on Microwave and Millimeter Wave Technology (ICMMT)*, Guangzhou, China, pp. 1-3, May 2019.

[76]   Y. Han, B. Zhu, and Z. Yan, "Design of a wave-absorbing frequency selective surface unit," *Cross Strait Quad-Regional Radio Science and Wireless Technology Conference*, Xuzhou, pp. 1-2, July 2018.

[77]   M. Saikia and K. Srivastava, "Design of thin broadband microwave absorber using combination of capacitive and circuit analog absorbers," *IEEE Indian Conference on Antennas and Propogation*, Hyderabad, India, pp. 1-4, Dec. 2018.

[78]   Yu Fu, L. Wu, Y. Zhang, and J. Mao, "A broadband graphene absorber with double Minkowski loops," *IEEE International Conference on Microwave and Millimeter Wave Technology*, Beijing, pp. 107-109, June 2016.

[79]   D. Kundu, A. Mohan, and A. Chakrabarty, "Design of a conductive FSS based ultrathin absorber using impedance analysis method of equivalent circuit model," *IEEE Indian Conference on Antennas and Propogation*, Hyderabad, India, pp. 1-4, Dec. 2018.

[80]   Bara Döken, M. Kartal and Ş. Balta, "A simple frequency selective absorber surface design," *9th International Conference on Recent Advances in Space Technologies*, Istanbul, Turkey, pp. 79-82, June 2019.

[81]   S. Guo, Y. Zhang, Y. He, L. Miao, and J. Jiang, "Design of a broadband and switchable absorber using an absorb/reflective FSS," *Photonics & Electromagnetics Research Symposium - Fall*, Xiamen, China, pp. 2144-2148, Dec. 2019.

[82]   S. Ghosh, S. Bhattacharyya, and K. Srivastava, "Design and analysis of a broadband single layer circuit analog absorber," *46th European Microwave Conference*, London, pp. 584-587, Oct. 2016.

[83]   Sofian Hamid, H. Shakhtour, B. Kambach, and D. Heberling, "Design and oblique incidence performance of a planar radome absorber, "*11th European Conference on Antennas and Propagation*, Paris, pp. 3806-3810, 19-24 March 2017.

[84]   Y. Tsuda, T. Yasuzumi, and O. Hashimoto, "Design of thin wave absorbers using closely placed divided conductive film and resistive film," *Asia-Pacific Microwave Conference*, Melbourne, pp. 1798-1801, Dec. 2011.

[85]   J. Colinge*, Silicon-on-Insulator technology: Materials to VLSI,* 3rd Ed., Springer, USA, 2004.

[86]   A. Amara and O. Rozeau, *Planar double-gate transistor: From technology to circuit*, Springer, Netherlands, 2009.

[87]   Douglas A. Pucknell, *Basic VLSI design*, Prentice-Hall, 1994.

[88]   S. M. Sze, *VLSI technology*, 2nd Ed., McGraw-Hill Education Limited, Oct. 2003.

[89]   Y. Cheng, K. Imai, M. C. Jeng, Z. Liu, K. Chen, C. Hu, "Modelling temperature effects of quarter micrometre MOSFET in BSIM3v3 for Circuit Simulation," *Semiconductor Science Technology,* Vol. 12, pp. 1349-1354, Nov. 1997.

[90]   W. Liu "BSIM3v3.2.2 MOSFET Model User Manual", Department of Electrical and Computer Engineering, University of California, Berkeley, 1999.

[91]   X. Xi, "BSIM4.3.0 MOSFET Model User Manual", Department of Electrical and Computer Engineering, University of California, Berkeley, 2003.

[92]   Nitin Sachdeva and Neeraj Julka, "Effect of temperature fluctuations on MOSFET characteristics," *IJECT*, vol. 2, March 2011.

[93]   X. Liao, H. Li, Y. Hu, Z. Huang, E. Song, and H. Xiao, "Analysis of SiC MOSFET dI/dt and its temperature dependence," *43rd Annual Conference of the IEEE Industrial Electronics Society*, Beijing, pp. 864-869, Nov. 2017

[94]   L. Atzeni and S. Manzini, "Effect of body bias on NBTI of PMOS," *IEEE Transactions on Device and Materials Reliability*, vol. 17, no. 2, pp. 399-403, June 2017.

[95]   Ayodele S. Oluwole and Viranjay M. Srivastava, "Smart antenna for wireless communication systems using spatial signal processing," *J. of Communications*, vol. 12, no. 6, pp. 328-339, June 2017.

[96]   Andre Prata, Sergio C. Pires, Mustafa Acar, Arnaldo S.Oliveira, and Nuno B. Carvalho, "Towards circulator-free multi antenna transmitters for 5G," *IEEE MTT-S International Microwave Symposium*, Honolulu, HI, USA, pp. 677-680, June 2017

[97]   N. Kaim Khani, Z. Chen, F. Yin, and H. Xing, "MU-MIMO Scheme: Single layer multi-user transmison," *Journal of Communications*, vol. 9, no. 5, pp. 411-418, May 2014.

[98]   Elliot O. Omoru and Viranjay M. Srivastava, "MOSFET based absorber of reflected signal in 5G massive MIMO base station - A circuit perspective," *Journal of Communication*, vol. 15, no. 11, Nov. 2020, in press.

[99]   Ahmed Moussa, Yaser Khalaf, and Ahmed Khalil, "Design of a novel circulator for wireless transceivers," *Int. Conf. on Microelectronics*, Cairo, Egypt, pp. 1-4, Dec. 2007.

[100] Chia H. Chang, Yu T. Lo, and Jean F. Kiang, "A 30 GHz active quasi-circulator with current-reuse technique in 0.18 µm CMOS technology," *IEEE Microwave and Wireless Components Letters*, vol. 20, no. 12, pp. 693-695, Dec. 2010.

[101] Edward A. Ohm, "A broad-band microwave circulator," *IRE Transactions on Microwave Theory and Techniques*, vol. 4, no. 4, pp. 210-217, Oct. 1956.

[102] Petri S. Heljo, Miao Li, Kaisa E. Lilja, Himadri S. Majumdar, and Donald Lupo, "Printed half-wave and full-wave rectifier circuits based on organic diodes," *IEEE Transactions on Electron Devices*, vol. 60, no. 2, pp. 870-874, Feb. 2013.

[103] Shohei Imai, Shoichi Tamaru, Kazuhiro Fujimori, Minoru Sanagi, and Shigeji Nogi, "Efficiency and harmonics generation in microwave to DC conversion circuits of half-wave and full-wave rectifier types," *IEEE MTT-S International Microwave Workshop Series on Innovative Wireless Power Transmission: Technologies, Systems, and Applications*, Kyoto Japan, pp. 15-18, May 2011

[104] Michael Roberg, Tibault Reveyrand, Ignacio Ramos, Erez A. Falkenstein, and Zoya Popovic, "High-efficiency harmonically terminated diode and transistor rectifiers," *IEEE Transactions on Microwave Theory and Techniques*, vol. 60, no. 12, pp. 4043-4052, Dec. 2012.

[105] Mike Golio, *RF and microwave semiconductor device handbook*, CRC Press, USA, 2003.

[106] Ravinder Kumar, Munish Kumar, and Viranjay M. Srivastava, "Design and noise optimization of RF low noise amplifier for IEEE standard 802.11a WLAN," *Int. J. of VLSI Design and Communication Systems*, vol. 3, no. 2, pp. 165-173, April 2012.

[107] Steve Winder, *Analog and Digital Filter Design*, 2nd Ed., Newnes, Elsevier, Oct. 2002.

[108] Viranjay M. Srivastava, K. S. Yadav, and G. Singh, "Double-pole four-throw RF CMOS switch design with double-gate transistors," *2010 Annual IEEE India Council Int. Conference (INDICON-2010),* India, pp. 1-4, Dec. 2010.

[109] Xiao P. Chen and Ke Wu, "Substrate Integrated Waveguide Filter," *IEEE Microwave Magazine*, vol. 15, no. 5, pp. 108-116, July - Aug. 2014.

[110] Negar Reiskarimian, Jin Zhou, and Harish Krishnaswamy, "A CMOS passive LPTV nonmagnetic circulator and its application in a full-duplex receiver," *IEEE Journal of Solid-State Circuits*, vol. 52, no. 5, pp. 1358 – 1372, May 2017.

[111] Viranjay M. Srivastava, K. S. Yadav, and G. Singh, "Explicit model of cylindrical surrounding double-gate MOSFETs," *WSEAS Trans. on Circuits and Systems,* vol. 12, no. 3, pp. 81-90, March 2013.

[112] Vadim Issakov, *Microwave circuits for 24 GHz automotive radar in Silicon-based technologies*, Springer, 2010.

[113] S. Chou, X. Wang, and F. Blaabjerg, "Stability analysis of grid-connected VSCs based on S-parameters and reflection coefficient," *IEEE Energy Conversion Congress and Exposition (ECCE),* Baltimore, MD, USA, pp. 5171-5178, 2019.

[114] Janusz Dobrowolski, *Scattering parameters in RF and microwave circuit analysis and design*, Artech, 2016.

[115] J. Castagnola, F. Dualibe, and H. García-Vázquez, "Using scattering parameters and the gm/ID MOST ratio for characterisation and design of RF circuits," *IEEE 59th International Midwest Symposium on Circuits and Systems (MWSCAS)*, Abu Dhabi, pp. 1-4, 2016.

[116] Pierre Jarry; Jacques Beneat, "Advanced design techniques and realizations of microwave and RF filters*," IEEE*, 2008.

[117] Yusuke Moriwaki, Takehiro Imura, and Yoichi Hori, "Basic study on reduction of reflected power using DC/DC converters in wireless power transfer system via magnetic resonant coupling," *2011 IEEE 33rd International Telecommunications Energy Conference (INTELEC)*, Amsterdam, Netherlands, 9-13 Oct. 2011, pp. 1-5.

[118] Aravind Nagulu, Andrea Alu, and Harish Krishnaswamy, "Fully-integrated non-magnetic 180 nm SOI circulator with > 1W P1dB, >+50dBm IIP3 and high isolation across 1.85 VSWR," *IEEE Radio Frequency Integrated Circuits Symposium (RFIC)*, Philadelphia, PA, USA, pp. 104-107, June 2018.

[119] Viranjay M. Srivastava, K. S. Yadav, and G. Singh, "Performance of double-pole four-throw double-gate RF CMOS switch in 45 nm technology," *Int. J. of Wireless Engineering and Technology*, vol. 1, no. 2, pp. 47-54, Oct. 2010.

[120] Aravind Nagulu and Harish Krishnaswamy, "Non-magnetic CMOS switched-transmission-line circulators with high power handling and antenna balancing: theory and implementation," *IEEE Journal of Solid-State Circuits*, vol. 54, no, 5, pp. 1288 – 1303, May 2019.

[121] Viranjay M. Srivastava, K. S. Yadav, and G. Singh, "Capacitive model and S-parameters of double-pole four-throw double-gate RF CMOS switch," *Int. J. of Wireless Engineering and Technology*, vol. 2, no. 1, pp. 15-22, Jan. 2011.

[122] Viranjay M. Srivastava, K. S. Yadav, and G. Singh, "Double pole four throw switch design with CMOS inverter," *5th IEEE Conf. on Wireless Communication and Sensor Networks (WCSN-2009)*, Allahabad, India, pp. 1-4, Dec. 2009,

[123] Zhong Chen, Hamid Bayat and Anoop Adhyapak, "Multiphysics analysis of RF pyramidal absorbers," *Antenna Measurement Techniques Association Symposium*, San Diego, CA, USA, pp. 1-6, 6-11 Oct. 2019

[124] Z. Chen, "Common RF absorbers evaluations in W-band (75-100 GHz)," *IEEE International Symposium on Electromagnetic Compatibility & Signal/Power Integrity*, Washington, DC, pp. 1-31, 2017.

NOTES